Inorg. Chem. **2008**, *47*, 2449−2463

Combined Ligand Field and Density Functional Theory Analysis of the Magnetic Anisotropy in Oligonuclear Complexes Based on Fe^{III}−CN−M^{II} Exchange-Coupled Pairs

Mihail Atanasov,*,†,‡,§ **Peter Comba**,*,‡ **and Claude A. Daul**§

Institute of General and Inorganic Chemistry, Bulgarian Academy of Sciences, Acad. Georgi Bontchev Str. Bl.11, 1113 Sofia, Bulgaria, Anorganisch-Chemisches Institut, Universität Heidelberg, Im Neuenheimer Feld 270, D-69120 Heidelberg, Germany, and Département de Chimie, Université de Fribourg, Ch. du Musée 9, CH-1700 Fribourg, Switzerland

Received August 30, 2007

Magnetic anisotropy in cyanide-bridged single-molecule magnets (SMMs) with Fe^{III}−CN−M^{II} (M = Cu, Ni) exchange-coupled pairs was analyzed using a density functional theory (DFT)-based ligand field model. A pronounced magnetic anisotropy due to exchange was found for linear Fe^{III}−CN−M^{II} units with fourfold symmetry. This results from spin–orbit coupling of the $[Fe^{III}(CN)_6]^{3-}$ unit and was found to be enhanced by a tetragonal field, leading to a ^2E_g ground state for Fe^{III}. In contrast, a trigonal field (e.g., due to τ_{2g} Jahn–Teller angular distortions) led to a reduction of the magnetic anisotropy. A large enhancement of the anisotropy was found for the Fe^{III}−CN−Ni^{II} exchange pair if anisotropic exchange combined with a negative zero-field splitting energy of the $S = 1$ ground state of Ni^{II} in tetragonally compressed octahedra, while cancellation of the two anisotropic contributions was predicted for tetragonal elongations. A recently developed DFT approach to Jahn–Teller activity in low-spin hexacyanometalates was used to address the influence of dynamic Jahn–Teller coupling on the magnetic anisotropy. Spin Hamiltonian parameters derived for linear Fe−M subunits were combined using a vector-coupling scheme to yield the spin Hamiltonian for the entire spin cluster. The magnetic properties of published oligonuclear transition-metal complexes with ferromagnetic ground states are discussed qualitatively, and predictive concepts for a systematic search of cyanide-based SMM materials are presented.

1. Introduction

The search for single-molecule magnets (SMMs), which are spin clusters with low-temperature blocking of the magnetization, has led to the synthesis and characterization of a large number of oligonuclear, cyanide-bridged complexes with low-spin Fe^{III} or Mn^{III} cyanides coupled to Cu^{II}, Ni^{II}, or Mn^{II}[1−21] (see ref 18 for a recent review). Ferromagnetic or uncompensated antiferromagnetic spin coupling takes place in these complexes and leads to ground states having large values of the spin quantum number, *S*. These states are split in zero field because the symmetry is lower than spherical. If the zero-field splitting parameter *D* is negative, sublevels with the highest spin momenta ($M_S = \pm S$) are stabilized relative to the other sublevels. The result is a bistability having an energy barrier *U* for reversal of the magnetization, where *U* is proportional to $S^2|D|$ or $(S^2 - {}^1/_4)|D|$ for molecules with integer or half-integer values of *S*, respectively. A thorough understanding of the factors which affect this splitting is crucial for the design of SMM materials.

* To whom correspondence should be addressed. Phone: (+49) 6221-548453. Fax: (+49) 6221-546617. E-mail: mihail.atanasov@aci.uni-heidelberg.de (M.A.), peter.comba@aci.uni-heidelberg.de (P.C.).
† Bulgarian Academy of Sciences.
‡ Universität Heidelberg.
§ Université de Fribourg.

(1) Li, D.; Clérac, R.; Parkin, S.; Wang, G.; Yee, G. T.; Holmes, S. M. *Inorg. Chem.* **2006**, *45*, 5251.
(2) Bartlett, B. M.; Harris, T. D.; DeGroot, M. W.; Long, J. R. Z. *Anorg. Allg. Chem.* **2007**, *633*, 2380.
(3) Gu, Z.-G.; Yang, Q.-F.; Liu, W.; Song, Y.; Li, Y.-Z.; Zuo, J.-L.; You, X.-Z. *Inorg. Chem.* **2006**, *45*, 8895.
(4) Li, D.; Parkin, S.; Wang, G.; Yee, G. T.; Clérac, R.; Wernsdorfer, W.; Holmes, S. M. *J. Am. Chem. Soc.* **2006**, *128*, 4214.
(5) Oshio, H.; Tamada, O.; Onodera, H.; Ito, T.; Ikoma, T.; Tero-Kubota, S. *Inorg. Chem.* **1999**, *38*, 5686.
(6) Oshio, H.; Yamamoto, M.; Ito, T. *Inorg. Chem.* **2002**, *41*, 5817.
(7) Li, D.; Parkin, S.; Wang, G.; Yee, G. T.; Prosvirin, A. V.; Holmes, S. M. *Inorg. Chem.* **2005**, *44*, 4903.

10.1021/ic701702x CCC: $40.75
Published on Web 02/27/2008

In this work, we studied the magnetic anisotropy in magnetic clusters of singly bridged $Fe^{III}-CN-M^{II}$ (M = Cu, Ni) pairs having a low-spin ground state for the $[Fe(CN)_6]^{3-}$ site. Previous density functional theory (DFT) calculations showed that a strictly linear $Fe^{III}-CN-Cu^{II}$ bridge with an octahedral $[Fe(CN)_6]^{3-}$ site induces strong anisotropy in the $S = 1$ ground state of the Cu−Fe pair.[22] This anisotropy emerges from unquenched orbital momenta in the $^2T_{2g}$ ground state of Fe^{III} and their mixing with the spin via first-order spin–orbit coupling. Therefore, the total spin of the cluster is an ill-defined quantity, and the isotropic exchange $-J\hat{\mathbf{s}}_1\cdot\hat{\mathbf{s}}_2$ breaks down. Jahn–Teller coupling within the $^2T_{2g}$ ground state of $[Fe(CN)_6]^{3-}$ is significant and governed by the activity of the τ_{2g} vibrational modes, which distort the octahedral geometry toward a trigonally compressed D_{3d} structure.[23,24] This distortion is large enough to induce anisotropy in the magnetic susceptibility and the **g** tensor, which leads to a consistent description of the experimental magnetic and spectroscopic data of $[Fe(CN)_6]^{3-}$ and $[Mn(CN)_6]^{3-}$.[24] We have now extended these studies to $Fe^{III}-CN-Cu^{II}$ and $Fe^{III}-CN-Ni^{II}$ exchange-coupled pairs and larger spin clusters built from these pairs.

Theoretical models for anisotropic exchange coupling have been an area of focus since the early days of magnetochemistry. The seminal work by Dirac[25] considered exchange contributions from different orbital pairs. Their importance for magnetic anisotropy was recognized by Van Vleck and Huang,[26–28] and the theory was further developed by Levy,[29,30] Lines,[31] Kahn,[32] and Drillon and Georges;[33] group-theoretical arguments for anisotropic exchange coupling were pioneered by Tsukerblat and co-workers.[34–39] Applications to various systems, such as $Ti_2Cl_9^{3-}$,[40–48] oxo-bridged triangular $Fe^{III}_2Co^{II}$,[38] cyano-bridged $Cr^{III}Fe^{II}$,[49] carboxylato-bridged dinuclear Co^{II},[50,51] trigonal bipyramidal cyano-bridged $Mn^{II}_2Mn^{III}_3$,[53–57] dinuclear $Yb_2Cl_9^{3-}$,[58] $Yb_2Br_9^{3-}$,[58] and $YbCrBr_9^{3-}$,[59,60] a $Cu^{II}-Fe^{III}$ pair with a low-spin porphyrin Fe^{III} center,[61–64] and spin–spin coupling in

(8) Liu, W.; Wang, C.-F.; Li, Y.-Z.; Zuo, J.-L.; You, X.-Z. *Inorg. Chem.* **2006**, *45*, 10058.
(9) Wang, C.-F.; Zuo, J.-L.; Bartlett, B. M.; Song, Y.; Long, J. R.; You, X.-Z. *J. Am. Chem. Soc.* **2006**, *128*, 7162.
(10) Gu, Z.-G.; Liu, W.; Yang, Q.-F.; Zhou, X.-H.; Zuo, J.-L.; You, X.-Z. *Inorg. Chem.* **2007**, *46*, 3236.
(11) Van Langenberg, K.; Batten, S. R.; Berry, K. J.; Hockless, D. C. R.; Moubaraki, B.; Murray, K. S. *Inorg. Chem.* **1997**, *36*, 5006.
(12) Berlinguette, C. P.; Galán-Mascarós, J. R.; Dunbar, K. R. *Inorg. Chem.* **2003**, *42*, 3416.
(13) Wang, S.; Zuo, J.-L.; Zhou, H.-C.; Choi, H. J.; Ke, Y.; Long, J. R.; You, X.-Z. *Angew. Chem., Int. Ed.* **2004**, *43*, 5940.
(14) Choi, H. J.; Sokol, J. J.; Long, J. R. *Inorg. Chem.* **2004**, *43*, 1606.
(15) Ni, W.-W.; Ni, Z.-H.; Cui, A.-L.; Liang, X.; Kou, H.-Z. *Inorg. Chem.* **2007**, *46*, 22.
(16) Ni, Z.-H.; Kou, H.-Z.; Zhang, L.-F.; Ni, W.-W.; Jiang, Y.-B.; Cui, A.-L. *Inorg. Chem.* **2005**, *44*, 9631.
(17) Berlinguette, C. P.; Vaughn, D.; Cañada-Vilalta, C.; Galán-Mascarós, J. R.; Dunbar, K. R. *Angew. Chem.* **2003**, *115*, 1561.
(18) Beltran, L. M. C.; Long, J. R. *Acc. Chem. Res.* **2005**, *38*, 325.
(19) Rodríguez-Diéguez, A.; Kivekäs, R.; Sillanpää, R.; Cano, J.; Lloret, F.; McKee, V.; Stoeckli-Evans, H.; Colacio, E. *Inorg. Chem.* **2006**, *45*, 10537.
(20) Toma, L. M.; Lescouëzec, R.; Pasán, J.; Ruiz-Pérez, C.; Vaissermann, J.; Cano, J.; Carrasco, R.; Wernsdorfer, W.; Lloret, F.; Julve, M. *J. Am. Chem. Soc.* **2006**, *128*, 4842.
(21) Toma, L. M.; Delgado, F. S.; Ruiz-Pérez, C.; Carrasco, R.; Cano, J.; Lloret, F.; Julve, M. *Dalton Trans.* **2004**, 2836.
(22) Atanasov, M.; Comba, P.; Daul, C. A. *J. Phys. Chem. A* **2006**, *110*, 13332.
(23) Atanasov, M.; Comba, P. *J. Mol. Struct.* **2007**, *838*, 157.
(24) Atanasov, M.; Comba, P.; Daul, C. A.; Hauser, A. *J. Phys. Chem. A* **2007**, *111*, 9145.
(25) Dirac, P. A. M. *Proc. R. Soc. London* **1929**, *A123*, 714.
(26) Van Vleck, J. H. *Rev. Mat. Fis. Teor., Univ. Nac. Tucumán* **1962**, *14*, 189.
(27) Van Vleck, J. H.; Huang, N. L. In *Polarisation Matière et Rayonnement*, Volume Jubilaire en l'Honneur d'Alfred Kastler; La Société Françaisede Physique, Ed.; Presses Universitaires de France: Paris, 1969; p 506.
(28) Huang, N. L.; Van Vleck, J. H. *J. Appl. Phys.* **1969**, *40*, 1144.
(29) Levy, P. M. *Phys. Rev.* **1969**, *177*, 509.
(30) Levy, P. M. In *Magnetic Oxides*; Craik, D. J., Ed.; John Wiley & Sons: London, 1975; p 181.
(31) Lines, M. E. *J. Chem. Phys.* **1971**, *55*, 2977.
(32) Kahn, O. *Mol. Phys.* **1975**, *29*, 1039.
(33) Drillon, M.; Georges, R. *Phys. Rev. B* **1981**, *24*, 1278.
(34) Tsukerblat, B. S.; Belinskii, M. I.; Fainzil'berg, V. E. *Sov. Sci. Rev.* **1987**, *B9*, 337.
(35) Borrás-Almenar, J. J.; Clemente-Juan, J. M.; Coronado, E.; Palii, A. V.; Tsukerblat, B. S. *J. Phys. Chem. A* **1998**, *102*, 200.
(36) Borrás-Almenar, J. J.; Clemente-Juan, J. M.; Coronado, E.; Tsukerblat, B. S. *Inorg. Chem.* **1999**, *38*, 6081.
(37) Borrás-Almenar, J. J.; Clemente-Juan, J. M.; Coronado, E.; Tsukerblat, B. S. *J. Comput. Chem.* **2001**, *22*, 985.
(38) Tsukerblat, B. S.; Palii, A. V.; Mirovitskii, V. Y.; Ostrovsky, S. M.; Turta, K.; Jovmir, T.; Shova, S.; Bartolome, J.; Evangelisti, M.; Filoti, G. *J. Chem. Phys.* **2001**, *115*, 9528.
(39) Palii, A. V.; Tsukerblat, B. S.; Coronado, E.; Clemente-Juan, J. M.; Borrás-Almenar, J. J. *J. Chem. Phys.* **2003**, *118*, 5566.
(40) Barraclough, C. G.; Gregson, A. K. *J. Chem. Soc., Faraday Trans.* **1972**, *2*, 177.
(41) Kahn, O. *Mol. Phys.* **1976**, *31*, 957.
(42) Briat, B.; Kahn, O.; Morgenstern-Badarau, I.; Rivoal, J. C. *Inorg. Chem.* **1981**, *20*, 4193.
(43) Drillon, M.; Georges, R. *Phys. Rev. B* **1982**, *26*, 3882.
(44) Leuenberger, B.; Güdel, H. U. *Mol. Phys.* **1984**, *51*, 1.
(45) Ceulemans, A.; Heylen, G. A.; Chibotaru, L. F.; Maes, T. L.; Pierloot, K.; Ribbing, C.; Vanquickenborne, L. G. *Inorg. Chim. Acta* **1996**, *251*, 15.
(46) Ceulemans, A.; Chibotaru, L. F.; Heylen, G. A.; Pierloot, K.; Vanquickenborne, L. G. *Chem. Rev.* **2000**, *100*, 787.
(47) Borrás-Almenar, J. J.; Clemente-Juan, J. M.; Coronado, E.; Palii, A. V.; Tsukerblat, B. S. *J. Chem. Phys.* **2001**, *114*, 1148.
(48) Borrás-Almenar, J. J.; Coronado, E.; Clemente-Juan, J. M.; Palii, A. V.; Tsukerblat, B. S. *J. Solid State Chem.* **2001**, *159*, 268.
(49) Palii, A. V.; Tsukerblat, B. S.; Verdaguer, M. *J. Chem. Phys.* **2002**, *117*, 7896.
(50) Ostrovsky, S. M.; Werner, R.; Brown, D. A.; Haase, W. *Chem. Phys. Lett.* **2002**, *353*, 290.
(51) Ostrovsky, S. M.; Falk, K.; Pelikan, J.; Brown, D. A.; Tomkowicz, Z.; Haase, W. *Inorg. Chem.* **2006**, *45*, 688.
(52) Palii, A. V.; Tsukerblat, B. S.; Coronado, E.; Clemente-Juan, J. M.; Borrás-Almenar, J. J. *Inorg. Chem.* **2003**, *42*, 2455.
(53) Palii, A. V.; Ostrovsky, S. M.; Klokishner, S. I.; Tsukerblat, B. S.; Berlinguette, C. P.; Dunbar, K. R.; Galán-Mascarós, J. R. *J. Am. Chem. Soc.* **2004**, *126*, 16860.
(54) Tsukerblat, B. S.; Palii, A. V.; Ostrovsky, S. M.; Kunitsky, S. V.; Klokishner, S. I.; Dunbar, K. R. *J. Chem. Theory Comput.* **2005**, *1*, 668.
(55) Palii, A. V.; Ostrovsky, S. M.; Klokishner, S. I.; Tsukerblat, B. S.; Dunbar, K. R. *ChemPhysChem* **2006**, *7*, 871.
(56) Ostrovsky, S. M.; Klokishner, S. I.; Palii, A. V.; Dunbar, K. R. *J. Mol. Struct.* **2007**, *838*, 138.
(57) Klokishner, S.; Ostrovsky, S.; Palii, A.; Dunbar, K. *J. Mol. Struct.* **2007**, *838*, 114.
(58) Palii, A. V.; Tsukerblat, B. S.; Clemente-Juan, J. M.; Coronado, E. *Inorg. Chem.* **2005**, *44*, 3989.
(59) Aebersold, M. A.; Güdel, H. U.; Hauser, A.; Furrer, A.; Blank, H.; Kahn, R. *Phys. Rev. B* **1993**, *48*, 12723.
(60) Mironov, V. S.; Chibotaru, L. F.; Ceulemans, A. *Phys. Rev. B* **2003**, *67*, 014424.
(61) Thomson, A. J.; Johnson, M. K.; Greenwood, C.; Gooding, P. E. *Biochem. J.* **1981**, *193*, 687.
(62) Thomson, A. J.; Greenwood, C.; Gadsby, P. M. A.; Peterson, J.; Eglinton, D. G.; Hill, B. C.; Nicholls, P. *J. Inorg. Biochem.* **1985**, *23*, 187.

molecular magnets based on the $[Mo(CN)_7]^{4-}$ complex[65–69] have been reported. Orbital degeneracy and strong spin–orbit coupling of Mo^{III} in the last of these led to an extremely anisotropic ground-state Kramers doublet of the Ising type.[67] Ideas concerning ways to control the magnetic anisotropy in oligonuclear complexes, based on simple angular overlap model[66,70] and extended Hückel[71] calculations, have been published. Anisotropic exchange has usually been described using perturbation theory with a modified version of the kinetic exchange model,[72,73] which involves metal-to-metal electron transfer processes mediated by the bridging ligands. However, ferromagnetic coupling described by potential exchange terms has usually been ignored by the kinetic exchange model, following a suggestion by Anderson.[72] Ab initio studies of magnetic anisotropy have been confined to single paramagnetic centers[74] or organic radicals[75] and, due to size constraints, only scarcely applied to oligonuclear transition-metal complexes.[45,46,76,77] Current DFT methods and perturbation theory for the computation of zero-field splitting in oligonuclear paramagnetic molecules[78–81] have restricted applicability in the case of orbital degeneracy or near-degeneracy, such as that encountered in the $Fe^{III}-Cu^{II}$ and $Fe^{III}-Ni^{II}$ exchange pairs discussed here.

We have developed a DFT-based ligand field theory (LFDFT)[82–85] that allows one to deduce in a parametric form all of the terms (i.e., the ligand field matrix,[83] Coulomb repulsion,[83] and spin–orbit coupling[86] terms) in the model Hamiltonian. LFDFT has been used to calculate optical spectra,[82,84] EPR g and hyperfine-coupling parameters,[87,88] both static and dynamic Jahn–Teller coupling[23,24,89,90] of mononuclear complexes, and isotropic magnetic exchange coupling in dinuclear transition-metal complexes.[91,92] We now describe an extension of this model to the anisotropic **g** and **D** tensors in dinuclear transition-metal complexes and show how coupling of the local $\mathbf{g}_i$ and single- ($\mathbf{D}_i$) and two-center ($\mathbf{D}_{ij}$) anisotropy tensors in oligonuclear cyanometalates can be used to discuss their anisotropic magnetic properties from first principles. The effect of spin–orbit coupling and static as well as dynamic Jahn–Teller coupling on the magnetic anisotropy of $Fe^{III}-Cu^{II}$ and $Fe^{III}-Ni^{II}$ exchange-coupled pairs is studied in detail. The new approach described in this work was used to qualitatively analyze published magnetic properties of spin clusters based on $Fe^{III}-Cu^{II}$ and $Fe^{III}-Ni^{II}$ exchange-coupled pairs with ferromagnetic ground states. On the basis of these results, predictive concepts for a systematic search of cyanide-based SMM materials are presented.

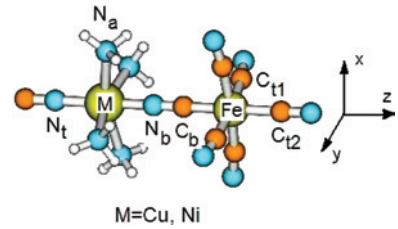

Figure 1. Model dinuclear complex of C_{4v} symmetry used for the calculation of the anisotropic exchange coupling. Atom labels used in the notation for the selected bond distances given in Table 2 are shown.

2. Theory

Here, we consider $Fe^{III}-CN-M^{II}$ exchange pairs having the geometry shown in Figure 1. The octahedral low-spin $[Fe(CN)_6]^{3-}$ site has a triply degenerate ground state ($^2T_{2g}$ in Griffith's notation,[93] with t_{2g} orbitals ξ, η, and ζ). When combined with the spins (α and β), this gives rise to six degenerate microstates, which are split by spin–orbit and Jahn–Teller coupling. In square planar complexes and tetragonally elongated or compressed octahedral complexes, there is a weak exchange coupling of these microstates, involving the $^2B_{1g}(d_{x^2-y^2})$ or $^2A_{1g}(d_{z^2})$ ground state of Cu^{II} in an $Fe^{III}-Cu^{II}$ pair or the $^3A_{2g}(d_{x^2-y^2}, d_{z^2})$ ground state of Ni^{II} in an $Fe^{III}-Ni^{II}$ pair. We consider the ground states of Cu^{II} and Ni^{II} to be well-defined and include all of the orbital effects on their spin ground states in the effective **g**-tensor values ($\mathbf{g}_2$), with positive deviations from the spin-only value ($g_0 = 2$), and in the zero-field splitting tensor $\mathbf{D}_2$ for Ni^{II}.

(63) Gunter, M. J.; Berry, K. J.; Murray, K. S. *J. Am. Chem. Soc.* **1984**, *106*, 4227.
(64) Bencini, A.; Gatteschi, D.; Zanchini, C. *Mol. Phys.* **1985**, *56*, 97.
(65) Larionova, J.; Gross, M.; Pilkington, M.; Andres, H.; Stoeckli-Evans, H.; Güdel, H. U.; Decurtins, S. *Angew. Chem., Int. Ed.* **2000**, *39*, 1605.
(66) Chibotaru, L. F.; Mironov, V. S.; Ceulemans, A. *Angew. Chem., Int. Ed.* **2001**, *40*, 4429.
(67) Mironov, V. S.; Chibotaru, L. F.; Ceulemans, A. *J. Am. Chem. Soc.* **2003**, *125*, 9750.
(68) You, S.; Ohkoshi, S.-I.; Arimoto, Y.; Seino, H.; Mizobe, Y.; Hashimoto, K. *Inorg. Chem.* **2003**, *42*, 1848.
(69) Ruiz, E.; Rajaraman, G.; Alvarez, S.; Gillon, B.; Stride, J.; Clérac, R.; Larionova, J.; Decurtins, S. *Angew. Chem., Int. Ed.* **2005**, *44*, 2711.
(70) Gatteschi, D.; Sorace, L. *J. Solid State Chem.* **2001**, *159*, 253.
(71) Atanasov, M.; Daul, C. A.; Güdel, H. U. In *Computational Chemistry: Reviews of Current Trends*; Leszczynski, J., Ed.; World Scientific: Singapore, 2005; Vol. 9, pp 153–194.
(72) Anderson, P. W. *Phys. Rev.* **1959**, *115*, 2.
(73) Moriya, T. *Phys. Rev.* **1960**, *120*, 91.
(74) Neese, F. *J. Am. Chem. Soc.* **2006**, *128*, 10213.
(75) Sinnecker, S.; Neese, F. *J. Phys. Chem. A* **2006**, *110*, 12267.
(76) Webb, S. P.; Gordon, M. S. *J. Chem. Phys.* **1998**, *109*, 919.
(77) Soda, T.; Kitagawa, Y.; Onishi, T.; Takano, Y.; Shigeta, Y.; Nagao, H.; Yoshioka, Y.; Yamaguchi, K. *Chem. Phys. Lett.* **2000**, *319*, 223.
(78) Pederson, M. R.; Khanna, S. N. *Phys. Rev. B* **1999**, *60*, 9566.
(79) Pederson, M. R.; Kortus, J.; Khanna, S. N. *J. Appl. Phys.* **2002**, *91*, 7149.
(80) Aquino, F.; Rodriguez, J. H. *J. Chem. Phys.* **2005**, *123*, 204902.
(81) Ribas-Arino, J.; Baruah, T.; Pederson, M. R. *J. Am. Chem. Soc.* **2006**, *128*, 9497.
(82) Atanasov, M.; Daul, C. A.; Rauzy, C. *Struct. Bonding* **2004**, *106*, 97–125.
(83) Atanasov, M.; Daul, C. A.; Rauzy, C. *Chem. Phys. Lett.* **2003**, *367*, 737.
(84) Atanasov, M.; Daul, C. A. *Chimia* **2005**, *59*, 504.
(85) Atanasov, M.; Daul, C. A.; Güdel, H. U.; Wesolowski, T.; Zbiri, M. *Inorg. Chem.* **2005**, *44*, 2954.
(86) Atanasov, M.; Rauzy, C.; Baettig, P.; Daul, C. A. *Int. J. Quantum Chem.* **2005**, *102*, 119.
(87) Atanasov, M.; Baerends, E. J.; Baettig, P.; Bruyndonckx, R.; Daul, C. A.; Rauzy, C.; Zbiri, M. *Chem. Phys. Lett.* **2004**, *399*, 433.
(88) Atanasov, M.; Daul, C. A.; Rohmer, M.-M.; Venkatachalam, T. *Chem. Phys. Lett.* **2006**, *427*, 449.
(89) Bruyndonckx, R.; Daul, C. A.; Manoharan, P. T.; Deiss, E. *Inorg. Chem.* **1997**, *36*, 4251.
(90) Reinen, D.; Atanasov, M.; Massa, W. *Z. Anorg. Allg. Chem.* **2006**, *632*, 1375.
(91) Atanasov, M.; Daul, C. A. *Chem. Phys. Lett.* **2003**, *379*, 209.
(92) Atanasov, M.; Daul, C. A. *Chem. Phys. Lett.* **2003**, *381*, 584.
(93) Griffith, J. S. *The Theory of Transition-Metal Ions*; Cambridge University Press: London, 1971.

Table 1. Symmetries of the Irreducible Tensor Operators $J\hat{\mathbf{s}}_1\cdot\hat{\mathbf{s}}_2$, $\hat{\mathbf{s}}_1\cdot\mathbf{D}\cdot\hat{\mathbf{s}}_2$, and $\hat{\mathbf{s}}_1\cdot\mathbf{A}\cdot\hat{\mathbf{s}}_2$ Spanned by the Direct Product of the Spin Operators $\hat{\mathbf{s}}_1$ and $\hat{\mathbf{s}}_2$ of Two Exchange-Coupled Ions in O_h and Its Subgroups, Consistent with a Linear Fe−CN−M Bridge with Fourfold Symmetry[a]

	O_h	C_{4v}	$C_{2v}[C_2, \sigma_v]$	C_2	$C_s[\sigma(xz)]$	$C_s[\sigma(yz)]$	$C_{2v}[C_2, \sigma_d]$	C_2	$C_s[\sigma(xz)]$	$C_s[\sigma(yz)]$
J	A_{1g}	**A_1**	**A_1**	**A**	**A′**	**A′**	**A_1**	**A**	**A′**	**A′**
D (symmetric)	E_g (diagonal)	**A_1**	**A_1**	**A**	**A′**	**A′**	**A_1**	**A**	**A′**	**A′**
		B_1	**A_1**	**A**	**A′**	**A′**	A_2	**A**	A″	A″
	T_{2g} (off-diagonal)	B_2	A_2	**A**	A″	A″	**A_1**	**A**	**A′**	**A′**
		E	$B_1 + B_2$	B + B	**A′** + A″	A″ + **A′**	$B_1 + B_2$	B + B	**A′** + A″	A″ + **A′**
A (antisymmetric)	T_{1g}	A_2	A_2	**A**	A″	A″	A_2	**A**	A″	A″
		E	$B_1 + B_2$	B + B	**A′** + A″	A″ + **A′**	$B_1 + B_2$	B + B	**A′** + A″	A″ + **A′**

[a] Totally symmetric representations which can yield nonzero matrix elements are rendered in bold text.

Table 2. Fe−C and M−N Bond Distances (in Å) from DFT Geometry Optimizations of the Model $[(CN)_5Fe-CN-M^{II}(CN)(NH_3)_4]^{2-}$ Complexes in Comparison with Experimental Structural Data (in Parentheses) for the M−NC−Fe Bridging Geometry in Closely Related Cu_3Fe_2 and Ni_3Fe_2 SMMs

M	R_{M-N_t}	R_{M-N_a}	R_{M-N_b}	R_{Fe-C_b}	$R_{Fe-C_{t1}}$	$R_{Fe-C_{t2}}$
Cu^{II}	1.949	2.434	1.918 (1.970[a])	1.867 (1.930[a])	1.978	1.972
Ni^{II}	2.026	2.214	1.969 (2.05[b])	1.865 (1.897[b])	1.984	1.977

[a] From ref 9. [b] From ref 2.

Under these conditions, the electronic states of the $Fe^{III}-M^{II}$ exchange pairs are described by the Hamiltonian in eq 1:

$$\hat{H} = \hat{H}_{SO} + \hat{H}_{LF} + \hat{H}_{exc} + \hat{H}_{Z1} + \hat{H}_{Z2} + \hat{H}_{SFS2} \qquad (1)$$

in which $\hat{H}_{SO} = \zeta_1\hat{\mathbf{l}}_1\cdot\hat{\mathbf{s}}_1$ and $\hat{H}_{LF}$ are the spin–orbit coupling and ligand field operators, respectively, for $[Fe(CN)_6]^{3-}$ and $\hat{H}_{Z1} = \mu_B(\hat{\mathbf{s}}_1 + k\hat{\mathbf{l}}_1)\cdot\mathbf{B}$ and $\hat{H}_{Z2} = \mu_B\hat{\mathbf{s}}_2\cdot\mathbf{g}_2\cdot\mathbf{B}$ are the Zeeman operators for $[Fe(CN)_6]^{3-}$ and M, respectively, where ζ_1 is the spin–orbit coupling constant for Fe^{III}, k is the covalency reduction factor, $\hat{\mathbf{s}}_1$ and $\hat{\mathbf{l}}_1$ are the spin and orbital angular momentum operators, respectively, for Fe^{III}, and $\hat{\mathbf{s}}_2$ is the spin angular momentum operator for M^{II}. $\hat{H}_{SFS2} = D_{Ni}(\hat{s}_{z2}^2 - {}^2/_3)$ is the operator which takes account of the possible single-center anisotropy in the $s_2 = 1$ ground state of Ni^{II}. The exchange coupling term $\hat{H}_{exc}$ in eq 1 accounts for the spins of Fe^{III} and M^{II} ($\hat{\mathbf{s}}_1$ and $\hat{\mathbf{s}}_2$, respectively) as well as the orbital degrees of freedom due to the degeneracy of the $^2T_{2g}$ ground state of $[Fe(CN)_6]^{3-}$, as shown in eq 2:

$$\hat{H}_{exc} = \sum_{\mu=\xi,\eta,\zeta} J_{\mu\mu}\hat{\mathbf{s}}_{1\mu}\cdot\hat{\mathbf{s}}_2 \qquad (2)$$

where $J_{\mu\mu}$ ($\mu = \xi, \eta, \zeta$) are the orbital exchange coupling constants between the spins $\mathbf{s}_{1\mu}$ of the singly occupied magnetic orbitals d_{yz} (ξ), d_{xz} (η), and d_{xy} (ζ) of Fe^{III} and the unpaired spins ($\mathbf{s}_2$) of M^{II}. In eq 2, we assume a C_{4v} pseudosymmetry for each $Fe^{III}-M^{II}$ pair with the local z axis along the $Fe^{III}-CN-M^{II}$ bridge (see Figure 1). This defines two exchange coupling parameters, $J_{\xi\xi} = J_{\eta\eta} \equiv J(E)$ and $J_{\zeta\zeta} \equiv J(B_2)$, for each $Fe^{III}-M^{II}$ pair, when the off-diagonal terms $J_{\mu\nu}(\mu \neq \nu)$ are neglected. The well-aligned magnetic orbitals ξ, η, and ζ and the matrices that represent all of the operators in eq 1 are then transformed using the eigenvectors of the ligand field operator $\hat{H}_{LF}$ on each center, in order to ensure invariance of the results with respect to the orbital rotations. The matrix that represents $\hat{H}_{LF}$ is given in a general form without any assumptions. It describes angular and radial distortions of each $[Fe(CN)_6{}^{3-}]$ unit of the oligonuclear cluster, which may arise from Jahn–Teller distortions, low-symmetry crystal packing effects, or asymmetry of the ligands. For the sake of the qualitative analysis presented here, we start with octahedral (O_h) $[Fe(CN)_6]^{3-}$ and restrict the treatment to a particular form of $\hat{H}_{LF}$, i.e., the operator $\hat{H}_{JT}$ for the Jahn–Teller effect that operates within the $^2T_{2g}$ ground state of $[Fe(CN)_6]^{3-}$. It has been shown that for the five Jahn–Teller-active ϵ_g and τ_{2g} vibrations, coupling of the $^2T_{2g}$ ground state of $[Fe(CN)_6]^{3-}$ to the trigonal modes τ_{2g} is dominant.[24] This leads to the stabilization of a D_{3d}-distorted $^2A_{1g}$ ground state derived from a trigonally compressed octahedron. Within the (ξ, η, ζ) orbital basis, the $\hat{H}_{LF}$ term in eq 1 is described by the matrix $\mathbf{H}_{JT}$ given in eq 3:

$$\mathbf{H}_{JT} = \begin{bmatrix} \frac{1}{2}K_\tau(Q_\xi^2 + Q_\eta^2 + Q_\zeta^2) & -V_\tau Q_\zeta & -V_\tau Q_\eta \\ -V_\tau Q_\zeta & \frac{1}{2}K_\tau(Q_\xi^2 + Q_\eta^2 + Q_\zeta^2) & -V_\tau Q_\xi \\ -V_\tau Q_\eta & -V_\tau Q_\xi & \frac{1}{2}K_\tau(Q_\xi^2 + Q_\eta^2 + Q_\zeta^2) \end{bmatrix} \qquad (3)$$

where Q_ξ, Q_η, and Q_ζ are the components of the τ_{2g} octahedral mode; V_τ is the linear vibronic coupling constant; and K_τ is the harmonic force constant. Terms which depend on V_τ describe the forces which distort the regular octahedral geometry, while the elastic force reflected by the harmonic term (i.e., the diagonal matrix elements of eq 3) tends to preserve it. An energy level diagram as a function of geometric distortion along the D_{3d} distortion pathway is presented in Figure 2. The ratio between the Jahn–Teller stabilization energy E_{JT} and the energy of the τ_{2g} vibration[94] (i.e., the vibronic coupling strength λ) is of importance for the treatment described below. Calculation of energy levels using eq 1 requires knowledge of all of the parameters of the model. An LFDFT-based procedure has been used to calculate the spin–orbit coupling constant,[86] the **g** tensors of Cu and Ni, the orbital reduction factor of Fe,[87] the orbital exchange parameters,[91,92] and the Jahn–Teller coupling constants.[24] The manifold of ground-state spin levels and excited states computed on the basis of eq 1 makes possible the interpretation of magnetic, EPR, and optical spectroscopic data.

We now focus on the spin levels of the electronic ground state and consider the coupling of the effective spin of Fe^{III}

(94) The Jahn−Teller stabilization energy and the energy of the τ_{2g} vibration are given by $E_{JT} = 2V_\tau{}^2/3K_\tau$ and $3\hbar\omega/2$, respectively, and have been found to be 135 and 140 cm^{-1}, respectively, in $[Fe(CN)_6]^{3-}$; see ref 24 for details.

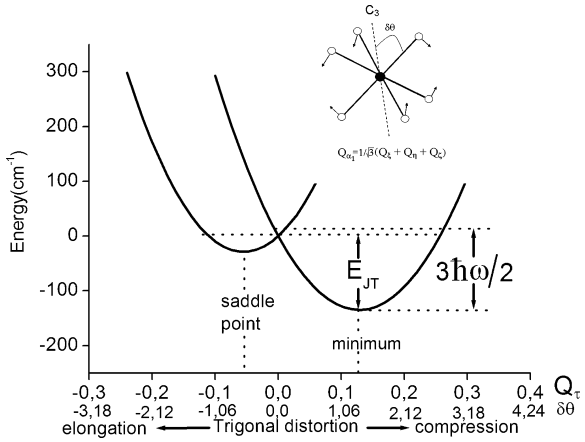

Figure 2. Cross section of the ground-state potential energy surface of $[Fe(CN)_6]^{3-}$ along the trigonal (1,1,1) and (−1,−1,−1) directions in the subspace of the τ_{2g} modes, which stabilize the $^2A_{1g}$ ground state (trigonal compression, absolute minimum) and ^2E_g excited state (trigonal elongation, saddle point), respectively. The Q_τ distortion (inset), the Jahn–Teller stabilization energy E_{JT}, and the zero-point vibrational energy $3\hbar\omega/2$ are shown. The following values of the vibronic coupling parameters[24] were used: $V_\tau = 1052$ cm^{-1}/Å, $K_\tau = 6069$ cm^{-1}/Å^2 (eq 3) and $3\hbar\omega/2 = 140$ cm^{-1}; also taken into account, but for the sake of simplicity not included in eq 3, were the second-order vibronic coupling terms $X_\tau = 449$ cm^{-1}/Å^2 and $L_\tau = 1584$ cm^{-1}/Å^2.

($s_1' = {}^1/_2$) with the real spin of Cu^{II} ($s_2 = {}^1/_2$) or Ni^{II} ($s_2 = 1$). This is described by the spin Hamiltonian given in eq 4:

$$\hat{H}_{sph} = -J\hat{\mathbf{s}}_1' \cdot \hat{\mathbf{s}}_2 + \hat{\mathbf{s}}_1' \cdot \mathbf{D}_{12} \cdot \hat{\mathbf{s}}_2 + \hat{\mathbf{s}}_2 \cdot \mathbf{D}_2 \cdot \hat{\mathbf{s}}_2 + \hat{\mathbf{s}}_1' \cdot \mathbf{A}_{12} \cdot \hat{\mathbf{s}}_2 + \mu_B \hat{\mathbf{s}}_1' \cdot \mathbf{g}_1 \cdot \mathbf{B} + \mu_B \hat{\mathbf{s}}_2 \cdot \mathbf{g}_2 \cdot \mathbf{B} \quad (4)$$

where J is the isotropic coupling constant, $\mathbf{D}_{12}$ and $\mathbf{A}_{12}$ are the traceless tensors for symmetric and antisymmetric exchange, respectively, $\mathbf{D}_2$ is the zero-field splitting tensor for Ni^{II}, and $\mathbf{g}_1$ and $\mathbf{g}_2$ are the effective $\mathbf{g}$ tensors for the $[Fe(CN)_6]^{3-}$ and Cu^{II} or Ni^{II} sites, respectively. The traceless symmetric exchange tensor $\mathbf{D}_{12}$ is

$$\mathbf{D}_{12} = \begin{bmatrix} D_{xx} & D_{xy} & D_{xz} \\ D_{xy} & D_{yy} & D_{yz} \\ D_{xz} & D_{yz} & -D_{xx} - D_{yy} \end{bmatrix} = \begin{bmatrix} -\frac{2}{3}D + 2E & D_{xy} & D_{xz} \\ D_{xy} & -\frac{2}{3}D - 2E & D_{yz} \\ D_{xz} & D_{yz} & \frac{4}{3}D \end{bmatrix} \quad (5)$$

where D and E are the axial and orthorhombic splitting parameters, respectively. The traceless antisymmetric exchange tensor $\mathbf{A}_{12}$ is

$$\mathbf{A}_{12} = \begin{bmatrix} 0 & A_z & -A_y \\ -A_z & 0 & A_x \\ A_y & -A_x & 0 \end{bmatrix} \quad (6)$$

There is a symmetry restriction for the number of independent nonzero components of $\mathbf{D}_{12}$ and $\mathbf{A}_{12}$: the spin operators $\hat{\mathbf{s}}_1'$ and $\hat{\mathbf{s}}_2$ transform according to the T_{1g} irreducible representation of the O_h point group, and the direct product $T_{1g} \otimes T_{1g}$ spans the symmetric irreducible representations A_{1g} ($\hat{\mathbf{s}}_1' \cdot \hat{\mathbf{s}}_2$), E_g ($\mathbf{D}_{12}$ diagonal terms), and T_{2g} ($\mathbf{D}_{12}$ off-diagonal terms) as well as the antisymmetric T_{1g} ($\mathbf{A}_{12}$) irreducible representation. Upon reduction to the main axes of the $\mathbf{D}_{12}$ tensor, only those components of $\mathbf{D}_{12}$ and $\mathbf{A}_{12}$ that are totally symmetric in O_h and its subgroups are nonzero. Thus, only J in O_h and only one parameter, D (which emerges from the diagonal elements of the $\mathbf{D}_{12}$ tensor in C_{4v}, the symmetry of a linear Fe−CN−M bridge), are nonzero (Figure 1 and Table 1). In this particular case, $\mathbf{D}_{12}$ assumes the simple form given by eq 7:

$$\mathbf{D}_{12} = \begin{bmatrix} -\frac{2}{3}D & 0 & 0 \\ 0 & -\frac{2}{3}D & 0 \\ 0 & 0 & \frac{4}{3}D \end{bmatrix} \quad (7)$$

It follows from the matrices of eqs 1 and 4 that all of the parameters can be determined. A similar approach to the exchange problem for a dinuclear Fe^{III}−CN−Cu^{II} complex has been described previously and applied to the important problem of the spin levels of a cyanide-bridged derivative of the enzyme cytochrome oxidase.[64] However, the large number of model parameters did not allow the method to be applied quantitatively at that time.

We now consider an oligonuclear cluster derived from Fe^{III}−Cu^{II} and Fe^{III}−Ni^{II} dinuclear building blocks. As long as there is a 1:1 mapping of the ground spin eigenstates of the Hamiltonians of eqs 1 and 4 (i.e., as long as the energy separation between the ground and excited electronic states is much larger than the exchange coupling energy, which is strictly valid for all of the cases considered here, as shown in the Supporting Information), the parameters of eq 4 can be determined, and the total Hamiltonian of the spin cluster is given by eq 8:

$$\hat{H}_{total} = \sum_{i \in \{Fe\}, j \in \{Cu\},\{Ni\}} [-J_{ij}\hat{\mathbf{S}}_i' \cdot \hat{\mathbf{S}}_j + \hat{\mathbf{S}}_i' \cdot (\mathbf{T}_{ij}\mathbf{D}_{ij}\mathbf{T}_{ij}^*) \cdot \hat{\mathbf{S}}_j + \hat{\mathbf{S}}_i' \cdot (\mathbf{T}_{ij}\mathbf{A}_{ij}\mathbf{T}_{ij}^*) \cdot \hat{\mathbf{S}}_j] + \sum_{j \in \{Cu\},\{Ni\}} [\hat{\mathbf{S}}_j \cdot (\mathbf{T}_j\mathbf{D}_j\mathbf{T}_j^*) \cdot \hat{\mathbf{S}}_j + \mu_B \hat{\mathbf{S}}_j \cdot (\mathbf{T}_j\mathbf{g}_j\mathbf{T}_j^*) \cdot \mathbf{B}] + \sum_{i \in \{Fe\}} \mu_B \hat{\mathbf{S}}_i' \cdot (\mathbf{T}_i\mathbf{g}_i\mathbf{T}_i^*) \cdot \mathbf{B} \quad (8)$$

where the single summations run over all of the Fe^{III}, Cu^{II}, and Ni^{II} ions (contained in the sets labeled {Fe}, {Cu}, and {Ni}, respectively); the double summation runs over all of the Fe^{III}−M^{II} pairs; $\mathbf{T}_i^*$, $\mathbf{T}_j^*$, and $\mathbf{T}_{ij}^*$ are the matrices which transform the local Cartesian axes (x_l, y_l, z_l) of each Fe^{III} and M^{II} magnetic center and each Fe^{III}−M^{II} exchange pair, respectively, into the global axes (x, y, z); and $\hat{\mathbf{S}}_i'$ and $\hat{\mathbf{S}}_j$ are the spin operators in the global frame. Application of this spin Hamiltonian operator to the basis composed of all possible products of single-ion spin functions produces Hermitian matrices having dimensions of 8 × 8 or 18 × 18, 16 × 16 or 36 × 36, 32 × 32 or 108 × 108, and 256 × 256 or 1296 × 1296 for (Cu or Ni)$_2$Fe, (Cu or Ni)$_2$Fe$_2$, (Cu or Ni)$_3$Fe$_2$, and (Cu or Ni)$_4$Fe$_4$, respectively. These matrices were diagonalized numerically using standard routines.

The ground-state potential energy surface of $[Fe(CN)_6]^{3-}$ is very flat. There are four minima having D_{3d} symmetry, which are only 135 cm^{-1} more stable than the minimum having regular octahedral symmetry (Figure 2).[24] Therefore, the geometry of the $Fe^{III}-CN-M^{II}$ pair may still have C_{4v} symmetry upon time averaging, but the dynamics of the system may populate all of the minima (this is the dynamic Jahn–Teller effect; see Figure S.3b in the Supporting Information). A limited number of studies have addressed the effect of dynamic Jahn–Teller coupling on the magnetic exchange coupling.[42,48,56,57,95] Dynamic Jahn–Teller coupling has been applied in order to analyze the temperature dependence of the magnetic anisotropy of $[Fe(CN)_6]^{3-}$,[24] and the same approach is applied here for the $Fe^{III}-CN-M^{II}$ exchange-coupled pairs. Details are given in the Supporting Information.

3. Computational Details

DFT computations were performed using the Amsterdam Density Functional program (ADF).[96] The LDA-VWN functional,[97] which is known to perform better than GGA for geometries, in particular for metal–ligand bond distances, was employed in all of the calculations. Large Slater-type orbital triple-ζ basis sets including one polarization function (p-type for H and d-type for C and N) and the frozen-core approximation (up to 3p for the metal ions and 1s for carbon and nitrogen) were used. The $Fe^{III}-CN-M^{II}$ model system is shown in Figure 1; Fe−C and M−N bond distances from DFT geometry optimizations compared reasonably well with those reported for analogous compounds (Table 2). The ground state of Cu^{II} was chosen to have a single electron in the d_{z^2} orbital, implying a tetragonally compressed geometry with maximum unpaired spin density directed toward Fe^{III}. For Ni^{II}, we chose a $^3A_{2g}$ ground state having two unpaired electrons in the e_g orbital ($d_{x^2-y^2}{}^1d_{z^2}{}^1$). Exchange coupling energies $J(^2E)$ and $J(^2B_2)$ were obtained from spin-polarized broken-symmetry DFT calculations, using both the spin-projected[98,99] and spin-unprojected[100–102] methods. Different functionals were tested, including the pure DFT functionals VWN,[97] PW91,[103,104] PBE,[105] and OPBE [which is a combination of Handy's optimized exchange (OPTX)[106] and the PBE correlation PBEc[105]] as well as hybrid functionals with various degrees of exact Hartree–Fock exchange, namely, the popular B3LYP[107] (20% HF) and its modifications with more (B1LYP,[108] 25% HF) or less (B3LYP*,[109,110] 15% HF) exchange (see discussions of the performance of these functionals,[111–115] the role of the self-interaction error,[116–118] and a new development[119]). Computed values of $J(^2E)$ and $J(^2B_2)$ (see Table S.1 in the Supporting Information) showed a strong dependence on the functional. Because of the orthogonality of the magnetic orbitals, i.e., σ for Cu^{II} and Ni^{II} and π for $[Fe(CN)_6]^{3-}$ (see Figure S.1 in the Supporting Information), a ferromagnetic exchange coupling was calculated in all cases [$J(^2E) > 0$]. We chose to use a B1LYP functional, which reproduced the correct order of magnitude of the exchange coupling energies (see Table S.1 in the Supporting Information). Alternative choices did not change the results qualitatively (see Figure S.4 in the Supporting Information). Values of $J(^2E)$ and $J(^2B_2)$ for the Fe−Cu and Fe−Ni pairs are listed in Table 3.

Table 3. Values of the Exchange Coupling Energies (in cm^{-1}) for the $Fe^{III}-CN-Cu^{II}$ Exchange Pair Obtained from Calculations Using the B1LYP Functional with Spin Projection and from Experiment, in Comparison with Corresponding Values Obtained for the $Fe^{III}-CN-Ni^{II}$ Exchange Pair[a]

electronic configuration of $[Fe(CN)_6]^{3-}$	$Fe^{III}-CN-Cu^{II}$		$Fe^{III}-CN-Ni^{II}$	
	calculated	experimental	calculated	experimental
$b_2{}^1e^4$	1.6	−	0	−
$b_2{}^2e^3$	19.4	17.0[b]	12.9	10.8, 9.7[c]

[a] In the calculations, the ground states of Cu^{II} in $Fe^{III}-CN-Cu^{II}$ and Ni^{II} in $Fe^{III}-CN-Ni^{II}$ were $d_{z^2}{}^1$ and $d_{x^2-y^2}{}^1d_{z^2}{}^1$, respectively. [b] Reported in ref 9 and obtained from a fit to magnetic susceptibility data for a Cu_3Fe_2 SMM in which the ground state of Cu was $d_{x^2-y^2}{}^1$. The value given here is twice that stated ref 9; multiplying their value by a factor of 2 was required because they included an extra factor of 2 in their definition of the exchange Hamiltonian. For comparison with the calculated result (in which the Cu ground state was $d_{z^2}{}^1$), this experimental energy must be multiplied by $2/\sqrt{3}$ [$J(d_{z^2}{}^1) = 2J(d_{x^2-y^2}{}^1)/\sqrt{3}$]. [c] Reported in refs 2 and 3, respectively, and obtained from fits to magnetic susceptibility data for Ni_3Fe_2 SMMs in which the ground state of Ni^{II} was $d_{x^2-y^2}{}^1d_{z^2}{}^1$.

4. Results and Discussion

4.1. Linear (C_{4v}) Dinuclear $Fe^{III}-CN-M^{II}$ Building Blocks with Octahedral $[Fe(CN)_6]^{3-}$ Sites. 4.1.1. The $Fe^{III}-CN-Cu^{II}$ Pair. The $^2T_{2g}$ ground state of $[Fe(CN)_6]^{3-}$ splits by spin–orbit coupling into a ground-state doublet

(95) Tsukerblat, B. S.; Vekhter, B. G. *Sov. Phys. Solid State* **1973**, *14*, 2204.
(96) Bérces, A.; Bo, C.; Boerrigter, P. M.; Cavallo, L.; Chong, D. P.; Deng, L.; Dickson, R. M.; Ellis, D. E.; Fan, L.; Fischer, T. H.; Fonseca Guerra, C.; van Gisbergen, S. J. A.; Groeneveld, J. A.; Gritsenko, O. V.; Grüning, M.; Harris, F. E.; van den Hoek, P.; Jacobsen, H.; van Kessel, G.; Kootstra, F.; van Lenthe, E.; McCormack, D. A.; Osinga, V. P.; Patchkovskii, S.; Philipsen, P. H. T.; Post, D.; Pye, C. C.; Ravenek, W.; Ros, P.; Schipper, P. R. T.; Schreckenbach, G.; Snijders, J. G.; Sola, M.; Swart, M.; Swerhone, D.; te Velde, G.; Vernooijs, P.; Versluis, L.; Visser, O.; van Wezenbeek, E.; Wiesenekker, G.; Wolff, S. K.; Woo, T. K.; Baerends, E. J.; Autschbach, J.; Ziegler, T. *ADF2006.01*; SCM, Theoretical Chemistry, Vrije Universiteit: Amsterdam, 2006 (http://www.scm.com).
(97) Vosko, S. H.; Wilk, L.; Nusair, M. *Can. J. Phys.* **1980**, *58*, 1200.
(98) Noodleman, L.; Norman, J. G., Jr *J. Chem. Phys.* **1979**, *70*, 4903.
(99) Noodleman, L. *J. Chem. Phys.* **1981**, *74*, 5737.
(100) Ruiz, E.; Cano, J.; Alvarez, S.; Alemany, P. *J. Comput. Chem.* **1999**, *20*, 1391.
(101) Ruiz, E.; Rodríguez-Fortea, A.; Cano, J.; Alvarez, S.; Alemany, P. *J. Comput. Chem.* **2003**, *24*, 982.
(102) Ruiz, E. *Struct. Bonding* **2004**, *113*, 71.
(103) Perdew, J. P.; Wang, Y. *Phys. Rev. B* **1986**, *33*, 8800.
(104) Perdew, J. P.; Chevary, J. A.; Vosko, S. H.; Jackson, K. A.; Pederson, M. R.; Singh, D. J.; Fiolhais, C. *Phys. Rev. B* **1992**, *46*, 6671.
(105) Perdew, J. P.; Burke, K.; Ernzerhof, M. *Phys. Rev. Lett.* **1996**, *77*, 3865. Perdew, J. P.; Burke, K.; Ernzerhof, M. *Phys. Rev. Lett.* **1997**, *78*, 1396. (Erratum).
(106) Handy, N. C.; Cohen, A. J. *Mol. Phys.* **2001**, *99*, 403.
(107) Becke, A. D. *J. Chem. Phys.* **1993**, *98*, 1372.
(108) Adamo, C.; Barone, V. *Chem. Phys. Lett.* **1997**, *274*, 242.
(109) Reiher, M.; Salomon, O.; Hess, B. A. *Theor. Chem. Acc.* **2001**, *107*, 48.
(110) Salomon, O.; Reiher, M.; Hess, B. A. *J. Chem. Phys.* **2002**, *117*, 4729.
(111) Stephens, P. J.; Devlin, F. J.; Chabalowski, C. F.; Frisch, M. J. *J. Phys. Chem.* **1994**, *98*, 11623.
(112) Reiher, M. *Inorg. Chem.* **2002**, *41*, 6928.
(113) Swart, M.; Groenhof, A. R.; Ehlers, A. W.; Lammertsma, K. *J. Phys. Chem. A* **2004**, *108*, 5479.
(114) Swart, M.; Ehlers, A. W.; Lammertsma, K. *Mol. Phys.* **2004**, *102*, 2467.
(115) Grüning, M.; Gritsenko, O. V.; Baerends, E. J. *J. Phys. Chem. A* **2004**, *108*, 4459.
(116) Ruiz, E.; Alvarez, S.; Cano, J.; Polo, V. *J. Chem. Phys.* **2005**, *123*, 164110.
(117) Adamo, C.; Barone, V.; Bencini, A.; Broer, R.; Filatov, M.; Harrison, N. M.; Illas, F.; Malrieu, J. P.; Moreira, I. d. P. R. *J. Chem. Phys.* **2006**, *124*, 107101.
(118) Ruiz, E.; Cano, J.; Alvarez, S.; Polo, V. *J. Chem. Phys.* **2006**, *124*, 107102.
(119) Zhao, Y.; Truhlar, D. G. *J. Phys. Chem. A* **2006**, *110*, 13126.

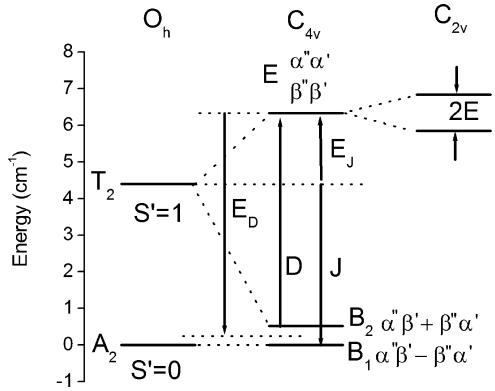

Figure 3. Spin energy levels and spin functions for the $Fe^{III}-CN-Cu^{II}$ exchange pair having C_{4v} symmetry. α' and β' are the spins of Cu^{II}, and α'' and β'' are the effective spins of Fe^{III}. The following parameter values were used for the C_{4v} energy levels: $J(^2E) = 19.4\ cm^{-1}$, $J(^2B_2) = 1.6\ cm^{-1}$, and $\zeta(Fe) = 345\ cm^{-1}$. The energy levels of the pair in O_h symmetry (obtained by collapsing the Cu^{II} and Fe^{III} nuclei) and the effect of an additional C_{2v} orthorhombicity are shown schematically.

$E''(\alpha'', \beta'')$ and an excited Kramers quartet $U'(\kappa, \lambda, \mu, \nu)$ that are separated by $3\zeta/2$, where $\zeta = 345\ cm^{-1}$[24] is the spin–orbit coupling constant of $[Fe(CN)_6]^{3-}$. In the C_{4v} symmetry of the linear Fe−CN−Cu unit, the $E''(\alpha'', \beta'')$ state transforms as $E''(\alpha'', \beta'')$ and couples via spin-exchange with the $E'(\alpha', \beta')$ spin state of Cu^{II} to give rise to a B_1 ground state and B_2 and E excited spin states (the notation used here for symmetry species follows ref 93). Expressions for the energies of these states in terms of the exchange coupling energies $J(^2E)$ and $J(^2B_2)$ defined above (derivations of which are provided in the Supporting Information) are given in eq 9:

$$\begin{aligned} E(B_1) &= -\frac{1}{6}J(^2E) - \frac{1}{12}J(^2B_2) \\ E(B_2) &= -\frac{1}{6}J(^2E) + \frac{1}{4}J(^2B_2) \\ E(E) &= \frac{1}{6}J(^2E) - \frac{1}{12}J(^2B_2) \end{aligned} \qquad (9)$$

Figure 3 visualizes these energy expressions and also lists the spin eigenfunctions. The spin ground state (B_1) is nonmagnetic. However, the B_2-B_1 energy separation [$J(^2B_2)/3$] is small, and the singly occupied a_1 orbital (d_{z^2}) of Cu interacts weakly with the magnetic b_2 orbital (d_{xy}) of δ-type Fe, resulting in a very small exchange energy of $J(^2B_2) = 1.6\ cm^{-1}$. This can be compared with the much larger energy, $J(^2E) = 19.4\ cm^{-1}$, arising from the σ/π interaction of the Cu a_1 (d_{z^2}) and Fe e (d_{xz},d_{yz}) orbitals. The latter places the E spin state above the ground state by $6.47\ cm^{-1}$. Calculations showed that configuration mixing of the ground-state spin levels (B_1, B_2, and E) with the excited-state levels [which result from the Cu^{II} a_1 (d_{z^2})−Fe^{III} $U'(\kappa, \lambda, \mu, \nu)$ exchange coupling] is vanishingly small (see the Supporting Information); nevertheless, we accounted for such mixing in all of the calculations. From a comparison of the numerical results with the eigenstates of the spin Hamiltonian $\hat{H}_{sph}$ (eq 4), the values of the parameters J, D (eq 7), $\mathbf{g}_1$ (for Fe), and $\mathbf{g}_2$ (for Cu) were deduced (eq 10).

$$\begin{aligned} J &= -\frac{2}{9}J(^2E) - \frac{1}{9}J(^2B_2) = -4.49\ cm^{-1} \\ D &= \frac{1}{3}J(^2E) - \frac{1}{3}J(^2B_2) = 5.94\ cm^{-1} \\ g_{1x} &= g_{1y} = g_{1z} = -\frac{2}{3} - \frac{4}{3}k = -1.72 \\ g_{2x} &= g_{2y} = 2.18; \quad g_{2z} = 2.00 \end{aligned} \qquad (10)$$

It is remarkable that in the dinuclear model, the local tensors $\mathbf{g}_1$ and $\mathbf{g}_2$ couple with different signs, leading to the interesting and unexpected result that the E term, which usually is ascribed to the magnetic $M_s = \pm 1$ pair in a ferromagnetically coupled pair with $s = {}^1/_2$ ions and has a negative value of D, is in this case highest in energy with small [for $g_z(E)$] or vanishing [for $g_{x,y}(E)$] **g**-tensor components (eq 11).

$$g_z(E) = g_{1z} + g_{2z} = 0.28; \quad g_{xy}(E) = 0 \qquad (11)$$

In contrast, the B_1 and B_2 states are composed of an equal admixture of $M_s = +1$ and $M_s = -1$ spin functions and are nonmagnetic. However, an external magnetic field **B** (with magnitude B) parallel to z leads to mixing of these states and thus tends to induce $M_s = +1$ (or $M_s = -1$) magnetic moments. Because the B_2-B_1 energy separation is small and the local tensors $\mathbf{g}_1$ (Fe) and $\mathbf{g}_2$ (Cu) couple with the same sign in the off-diagonal Zeeman term (eq 12), even weak magnetic fields can induce magnetic behavior.

$$\mathbf{H}(B_1, B_2) = \begin{bmatrix} 0 & \mu_B(-g_{1z} + g_{2z})B \\ \mu_B(-g_{1z} + g_{2z})B & \frac{1}{3}J(^2B_2) \end{bmatrix} \qquad (12)$$

This is shown by the dependence of the energies of these states on the magnetic field parallel and perpendicular to the z axis of the dinuclear model (Figure 4). A strong anisotropy with an easy axis oriented in the z direction is predicted. Therefore, if the rate of magnetic relaxation is small [i.e., if

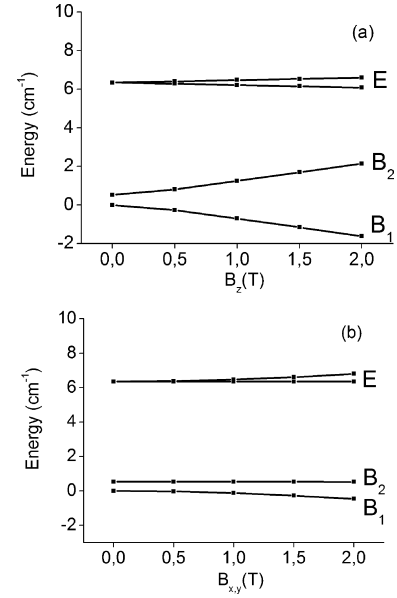

Figure 4. Energies of the spin states of the $Fe^{III}-CN-Cu^{II}$ pair in a magnetic field (a) parallel and (b) perpendicular to the bridging z axis. The following parameter values were used: $k(Fe) = 0.79$,[24] $g_{xy}(Cu) = 2.18$, and $g_z(Cu) = 2.000$ (values of the other parameters were the same as in Figure 3).

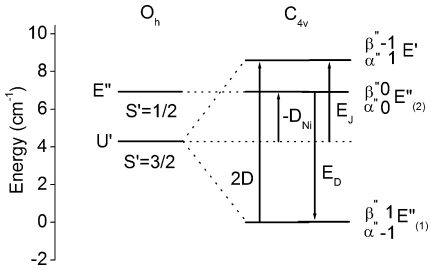

Figure 5. Spin energy levels and spin functions for the $Fe^{III}-CN-Ni^{II}$ exchange pair of C_{4v} symmetry. The values ±1 and 0 are the spins of Ni^{II}, and α″ and β″ are the effective spins of Fe^{III}. The following parameters were used for the C_{4v} energy levels: $J(^2E) = 12.9\ cm^{-1}$, $J(^2B_2) = 0\ cm^{-1}$, and $\zeta(Fe) = 345\ cm^{-1}$. The energy levels of the pair in O_h symmetry (obtained by collapsing the Ni^{II} and Fe^{III} nuclei) and the effect of the zero-field splitting of Ni^{II} ($D_{Ni} = -2.63\ cm^{-1}$) on the spin energy gap parameter $-E_D$ are also shown.

the rate is mediated by phonons (a "phonon bottleneck")], single-molecule magnetic behavior in a given time frame and in an applied external magnetic field may result. We refer to such a situation as a single-molecule metamagnet (SMMM).

It is worth noting that because of the unusual coupling of the $\mathbf{g}_1$ and $\mathbf{g}_2$ tensors, the calculated values of J and D have signs opposite to those conventionally assumed ($J > 0$, $D < 0$). It is interesting to note that a positive value of D (10.16 cm^{-1}) was observed in inelastic neutron scattering experiments on the dinuclear complex $Br_3Yb^{III}Br_3Cr^{III}Br_3$ with ferromagnetic $Yb^{III}-Cr^{III}$ coupling.[59] Because of the unusual signs of D and J, the energies E_D and E_J have been introduced in Figure 3. We use them in analogy to the well-known quantities U and J.

The large magnetic anisotropy in linear $Fe^{III}-CN-Cu^{II}$ pairs is consistent with qualitative results obtained for $Mo^{III}-CN-Mn^{II}$ pairs having the same bridging geometry using the kinetic exchange model, which takes into account both Ising-like ($\hat{S}_{Mo}\hat{S}_{Mn}$) and isotropic ($\hat{\mathbf{S}}_{Mo}\cdot\hat{\mathbf{S}}_{Mn}$) exchange terms.[67] Similar results obtained for $Cr^{III}-CN-Fe^{II}$ pairs using the same model have been reported.[49]

4.1.2. The $Fe^{III}-CN-Ni^{II}$ Pair. The E″(α″, β″) ground state of Fe^{III} couples with the $S = 1$ spin of Ni^{II}, giving rise to three Kramers doublets: the ground state, $E''_{(1)}$, and two excited spin states, $E''_{(2)}$ and E′. Expressions for the energies of these states in terms of the exchange coupling energies $J(^2E)$ and $J(^2B_2)$ and the Ni^{II} zero-field splitting energy D_{Ni} are given in eq 13 (complete matrices are given in the Supporting Information).

$$\begin{aligned} E(E''_{(1)}) &= -\frac{1}{3}J(^2E) + \frac{1}{6}J(^2B_2) + \frac{1}{3}D_{Ni} \\ E(E''_{(2)}) &= -\frac{2}{3}D_{Ni} \\ E(E') &= \frac{1}{3}J(^2E) - \frac{1}{6}J(^2B_2) + \frac{1}{3}D_{Ni} \end{aligned} \qquad (13)$$

An energy diagram for these states is shown in Figure 5, which also lists the spin eigenfunctions. In contrast to the $Fe^{III}-Cu^{II}$ pair, all of the spin states of the $Fe^{III}-Ni^{II}$ pair are doubly degenerate because of the odd number of spins (Kramers degeneracy). As for Cu^{II}, there is an in-phase coupling of the local tensors $\mathbf{g}_1$ (Fe) and $\mathbf{g}_2$ (Ni) in the $E''_{(1)}$ ground state and an out-of-phase coupling in the E′ excited spin state. As shown by the dependence of the energies of these states on the magnetic field parallel and perpendicular to the z axis of the pair (Figure 6), a strong anisotropy in the z direction is predicted. From the computed DFT values of $J(^2E)$ and $J(^2B_2)$ (12.9 and 0 cm^{-1}, respectively), eq 10 gave the values $J = -2.87\ cm^{-1}$ and $D = 4.30\ cm^{-1}$ for the parameters of the spin Hamiltonian (eq 4). As in the case of the $Fe^{III}-Cu^{II}$ pair, the quantities $-E_D$ and E_J can be defined and used in analogy to U and J to quantify the anisotropic and isotropic energy gaps, respectively (Figure 5). Both of the exchange terms as well as the single-ion zero-field splitting (D_{Ni}) affect the value of $-E_D$ (eq 14).

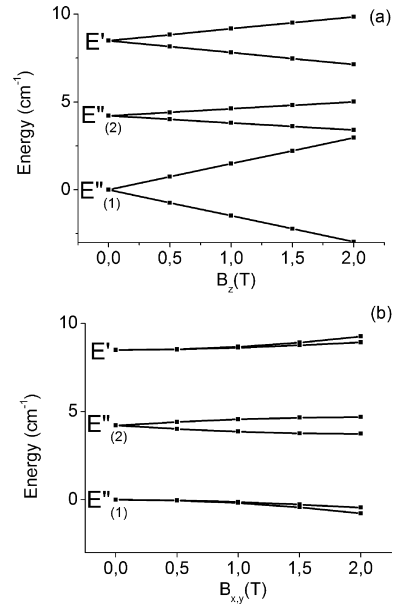

Figure 6. Zeeman splitting of the spin levels of the $Fe^{III}-CN-Ni^{II}$ pair in a magnetic field (a) parallel and (b) perpendicular to the bridging z axis. The following parameters were used: $k(Fe) = 0.79$, $g_{x,y,z}(Ni) = 2.30$, and $D_{Ni} = 0$ (values of the other parameters were the same as in Figure 5).

$$-E_D = \frac{1}{3}J(^2E) - \frac{1}{6}J(^2B_2) - D_{Ni} \qquad (14)$$

The parameter D_{Ni} is known to vary over a wide range, from positive values (e.g., 9.47 cm^{-1} [120]) in tetragonally elongated octahedra of Ni^{II} to negative values (e.g., −6.1 cm^{-1} [121]) in compressed octahedral structures.[122–124] Therefore, the anisotropy gap $-E_D$ (calculated using DFT to be 4.3 cm^{-1} due to exchange-only contributions) can largely be tuned by ligand-enforced distortions within the $Ni^{II}N_6$ building block. A reduction or enhancement of this energy is predicted for positive or negative values of D_{Ni}, respec-

(120) Boča, R.; Baran, P.; Dlháň, L.; Hvastijová, M.; Wltschek, G. *Chem. Phys. Lett.* **1998**, *284*, 254.
(121) Waldmann, O.; Hassmann, J.; Müller, P.; Volkmer, D.; Schubert, U. S.; Lehn, J.-M. *Phys. Rev. B* **1998**, *58*, 3277.
(122) Care must be taken to correlate the sign of D with the type of tetragonal distortion of $Ni^{II}L_6$. A negative value of D ($-22.34\ cm^{-1}$) has been reported in bis(acetato-*O*)tetrakis(imidazole-*N3*)Ni^{II} having an elongated tetragonal bipyramidal geometry and was attributed to different orbital reduction factors for axial (acetate) and equatorial (imidazole) ligands: Boča, R.; Dlháň, L.; Haase, W.; Herchel, R.; Maslejová, A.; Papánková, B. *Chem. Phys. Lett.* **2003**, *373*, 402.
(123) Boča, R. *Coord. Chem. Rev.* **2004**, *248*, 757.
(124) Boča, R. *Struct. Bonding* **2006**, *117*, 1.

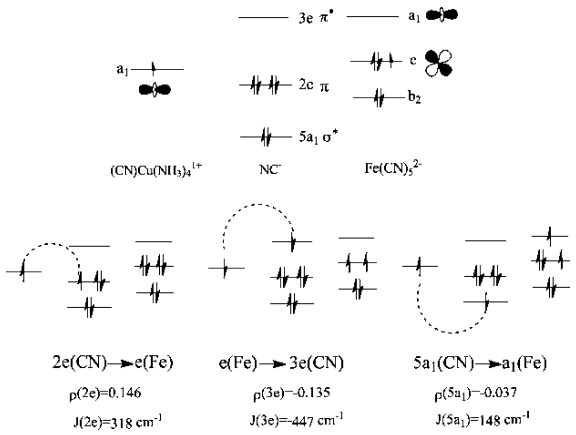

Figure 7. (top) Ground-state configuration and (bottom) configurations obtained via charge transfer to or from the occupied e (t_{2g}) or empty a_1 (e_g) orbitals of Fe^{III} [labeled using C_{4v} (O_h) symmetry notation], which induce spin densities on the CN^- bridging ligand. Coupling of the spins of CN in the charge-transfer configurations with the single spin on Cu^{II} is illustrated.

tively, assuming that the axes of the tetragonal tensors $\mathbf{D}_{Ni-Fe}$ and $\mathbf{D}_{Ni}$ are parallel. This is the case for octahedral Ni^{II} structures with tetragonal elongations (reduction of $-E_D$) or compressions (enhancement of $-E_D$).

4.1.3. Origin of the Magnetic Anisotropy in Fe−CN−M Pairs. The large magnetic anisotropy of the Fe−CN−M pairs is intrinsically related to the unquenched orbital moments of the $^2T_{2g}(\xi, \eta, \zeta)$ ground state of Fe^{III}, whose ξ and η components have the proper symmetry for an Fe−M exchange pathway to emerge via the π orbitals of CN^-. The $M_L = \pm 1$ orbital moments play a particularly important role for the spin levels. As seen in eqs 10 and 14, the magnetic anisotropy is dominated by $J(^2E)$. As $J(^2E)$ is obtained from DFT, it is a complex, many-electronic quantity, which includes various charge transfer excitations starting from the nominal purely ionic ground-state configuration (Figure 7). These include electronic transitions from (to) the fully occupied (empty) π bonding (antibonding) orbitals 2e (3e) of CN^-, which create α (β) spin densities on CN^-, and from the σ orbital $5a_1$ of CN^-, which lead to a β spin density on that orbital. An energy decomposition analysis of $J(^2E)$ described elsewhere[22] shows that the $2e(CN) \rightarrow e(Fe)$ and $5a_1(CN) \rightarrow a_1(Fe)$ donations dominate the sign of the $J(^2E)$ ferromagnetic coupling energy, while the $e(Fe) \rightarrow 3e(CN)$ back-donation yields a large but negative contribution which reduces $J(^2E)$.

4.2. Effect of Jahn–Teller Distortions of the $[Fe(CN)_6]^{3-}$ Site. 4.2.1. Static Jahn–Teller Distortions. The spin levels of Fe^{III}−CN−Cu^{II} and Fe^{III}−CN−Ni^{II} pairs change significantly when Jahn–Teller distortions along the trigonal axes of the octahedral $[Fe(CN)_6]^{3-}$ site are superimposed on the C_{4v} symmetry (Figure 8). There are four possible pathways for these distortions, which correlate with the body diagonals of the cube inscribed in the $[Fe(CN)_6]^{3-}$ octahedron (see Figure S3.b in the Supporting Information). The trigonal distortion along the $x = y = z$ direction (defined by $Q_\tau = Q_\xi = Q_\eta = Q_\zeta$ and visualized in the inset of Figure 2) reduces the C_{4v} symmetry toward C_s, with a symmetry plane that bisects the coordinate axes in the $x = y$ ($-x = -y$) direction and parallel to z. In agreement with the decrease in symmetry, the excited E spin state of the Fe−Cu pair splits, and its A″ component approaches the lower-lying A′ and A″ spin states. With greater distortion (increasing Q_τ), and concomitant quenching of the orbital angular momentum due to the $C_{4v} \rightarrow C_s$ symmetry reduction, the pattern of a ground-state spin triplet (split in zero field) and an excited-state singlet of the ferromagnetic Fe^{III}−Cu^{II} pair gradually starts to emerge (Figure 8a). This effect is much stronger for trigonal compression (leading to the energy minimum of the ground-state potential energy surface) than for trigonal elongation. Likewise, upon Q_τ distortion, the excited $E''_{(2)}$ spin state of the Fe^{III}−Ni^{II} pair drops in energy and approaches the $E''_{(1)}$ ground state, i.e., the zero-field-split $S = {}^3/_2$ ground-state quartet and the $S = {}^1/_2$ excited-state doublet are formed. Therefore, Jahn–Teller distortions tend to restore the usual spin coupling scheme in $s_1 = s_2 = {}^1/_2$ and $s_1 = {}^1/_2$, $s_2 = 1$ ferromagnetically coupled pairs. The anisotropic and isotropic gap energies $-E_D$ and E_J, respectively, which are indicated in Figure 8, manifest these changes in an impressive way. Upon distortion, $-E_D$ decreases and E_J increases for both Fe^{III}−Cu^{II} (Figure 9) and Fe^{III}−Ni^{II} (Figure 10). Figure 10 compares the cases of tetragonal compression (negative values of the zero-field splitting energy D_{Ni}) and tetragonal elongation (positive values of D_{Ni}) of the $S = 1$ ground state of the octahedral Ni^{II} complex with the case of no distortions around Ni^{II}. In these calculations, we have assumed that the tetragonal axes of Ni^{II} and the Fe−CN−Ni bridge of the Fe^{III}−Ni^{II} pair are parallel. Negative values of D_{Ni} lead to a drastic increase of the anisotropy, while positive values lead to a partial or

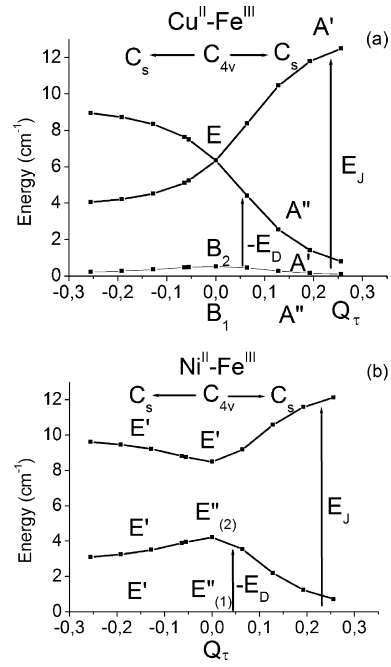

Figure 8. Effect of trigonal (τ_{2g}) Jahn–Teller distortions along the (1, 1, 1) ($Q_\tau > 0$, trigonal compression) and (−1, −1, −1) ($Q_\tau < 0$, trigonal elongation) directions on the spin energy levels of (a) Fe^{III}−Cu^{II} and (b) Fe^{III}−Ni^{II}. The values of the vibronic coupling constants for $[Fe(CN)_6]^{3-}$ used here were the same as in Figure 2, and values of the other parameters were the same as in Figure 3 (for Fe^{III}−Cu^{II}) or Figure 5 (for Fe^{III}−Ni^{II}, $D_{Ni} = 0$).

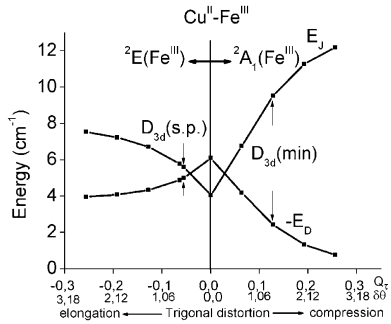

Figure 9. Effect of trigonal Jahn–Teller distortions on the spin energy gap parameters $-E_D$ and E_J for the $Fe^{III}-Cu^{II}$ pair. Values of $-E_D$ and E_J at the minimum and saddle point of the ground-state potential energy surface of $[Fe(CN)_6]^{3-}$ are indicated by arrows. Parameter values used were the same as in Figure 8a.

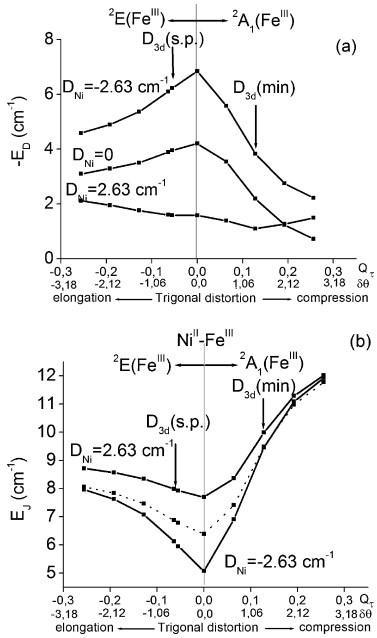

Figure 10. Effect of trigonal Jahn–Teller distortions on the spin energy gap parameters (a) $-E_D$ and (b) E_J for the $Fe^{III}-Ni^{II}$ pair. Values of $-E_D$ and E_J at the minimum and saddle point of the ground-state potential energy surface of $[Fe(CN)_6]^{3-}$ are indicated by arrows. Parameter values used were the same as in Figure 8b. The effect of the Ni zero-field splitting is shown (with $D_{Ni} = 2.63$ cm^{-1}, as in ref 131); the dotted curve for E_J refers to $D_{Ni} = 0$.

complete cancellation of the contributions to $-E_D$. The energy E_J is also affected by D_{Ni} in a significant way (Figure 10b).

It should be noted that the auxiliary quantities $-E_D$ and E_J have only been introduced for the purpose of interpretation, i.e., to quantify the information described by as many as nine parameters [J and the parameters in eqs 5 and 6 that define the tensors $\mathbf{D}_{12}$ and $\mathbf{A}_{12}$ in the exchange coupling operator (eq 4)]. In Table 4 we list these parameters for the $Fe^{III}-Cu^{II}$ and $Fe^{III}-Ni^{II}$ pairs, both without Jahn–Teller distortions ($Q_\tau = 0$) and with the distortion that corresponds to the trigonal minimum of $[Fe(CN)_6]^{3-}$ ($Q_\tau = 0.128$ Å). As the symmetry decreases from C_{4v} to C_s, as many as nine different parameters result, in agreement with the general orientation of the $\mathbf{D}_{12}$ and $\mathbf{A}_{12}$ tensors within the adopted global Cartesian frame. These can be reduced to the five independent parameters J, D, E, A_x, and A_y in the coordinate frame in which $\mathbf{D}_{12}$ is diagonal [see Table 1, $C_{4v} \rightarrow C_{2v}(C_2, \sigma_d) \rightarrow C_s$]; values of these five parameters are given in Table 4 for the $Fe^{III}-Ni^{II}$ pair. As expected, D is negative ($D = -6.09$ cm^{-1}, see Figure 10a), with main axes of $\mathbf{D}_{12}$ which undergo a specific rotation as a result of the Q_τ activity (see Table 4). A very pronounced orthorhombic component ($E = 0.77$ cm^{-1}) emerges along with significant antisymmetric exchange ($A_x = -0.29$ cm^{-1}, $A_y = -1.12$ cm^{-1}) due to Dzialoshinski−Moriya exchange coupling. This needs to be taken into account when modeling the magnetic properties.

4.2.2. Dynamic Jahn–Teller Distortions. Dynamic distortions related to the very flat ground-state potential energy surface of $[Fe(CN)_6]^{3-}$ with trigonal (D_{3d}) minima, which are only 135 cm^{-1} more stable than the nondistorted O_h geometry, induce specific changes in the spin coupling parameters of the $Fe^{III}-Ni^{II}$ pair, which we consider here as an example. Similar behavior has been calculated for the $Fe^{III}-Cu^{II}$ pair. As shown by the dependence of the energy $-E_D$, the anisotropy decreases as the vibronic coupling strength $\lambda = E_{JT}/(3\hbar\omega/2)$ increases (Figure 11). Calculations have shown that the dynamic Jahn–Teller coupling (λ) is small for $[Fe(CN)_6]^{3-}$, and its effect on $-E_D$ is very small. Also, there is no strong interplay between the anisotropy of Ni^{II} (D_{Ni}) and the dynamic Jahn–Teller coupling. However, the effect of λ on the magnetic anisotropy is significant for the isoelectronic $[Mn(CN)_6]^{4-}$ ion, for which a much stronger vibronic coupling has been predicted.[24] Dynamic Jahn–Teller coupling also tends to decrease the anisotropy of the **g** tensor of the $Fe^{III}-Ni^{II}$ pair. As λ increases, the large g_z component decreases while g_x and g_y [which are zero in C_{4v} and in the static Jahn–Teller coupling limit (see Table 4)] start to increase. The effect of dynamic Jahn–Teller coupling is found to be particularly pronounced when the exchange anisotropy (D) and the Ni^{II} single-ion anisotropy (D_{Ni}) counteract each other, i.e., when D and D_{Ni} have different signs.

4.3. Influence of Strain on the Magnetic Anisotropy. Strain effects due to an asymmetric ligand sphere or crystal packing forces can split the Fe^{III} $^2T_{2g}$ ground state and modify the magnetic anisotropy. Strains having the symmetries of the components of the τ_{2g} normal mode are formally described by a matrix of the form of eq 3, with a single energy parameter S_τ (the radial strain, which replaces V_τ) and angular distortions Q^s_ξ, Q^s_η, and Q^s_ζ (angular strains, which replace Q_ξ, Q_η, and Q_ζ, respectively); these are usually known from crystal structure data. Here we restrict our attention to strain having trigonal symmetry (C_3, $Q^s_\tau = Q^s_\xi = Q^s_\eta = Q^s_\zeta$). Its effect on the magnetic anisotropy for $Fe^{III}-Cu^{II}$ and $Fe^{III}-Ni^{II}$ pairs is qualitatively reflected by Figures 9 and 10a, respectively. These changes may be very large ($S_\tau \gg V_\tau$) and therefore induce partial or complete quenching of the magnetic anisotropy. With angular strain alone ($S_\tau = V_\tau$), quenching of orbital momenta due to trigonal compressions is predicted to be stronger than that due to trigonal elongation. The reduction of the magnetic anisotropy is due to the symmetry reduction ($C_s = C_{4v} + D_{3d}$), which leads to a complete loss of orbital degeneracy. This is not necessarily the case for tetragonal (D_{4h}) strain having a C_4 axis that

Table 4. Values (in cm^{-1}) of the Parameters in the Exchange Hamiltonians for $Fe^{III}-CN-Cu^{II}$ and $Fe^{III}-CN-Ni^{II}$ Exchange Pairs Having Jahn–Teller-Distorted $[Fe(CN)_6]^{3-}$ Octahedra Corresponding to the Minima of D_{3d} Symmetry[a] on the Ground-State Potential Energy Surface[b,c]

	J	D	E	D_{xy}	D_{xz}	D_{yz}	A_x	A_y	A_z
				$Fe^{III}-Cu^{II}$					
$Q_\tau = 0$[b]	−4.13	6.20	0	0	0	0	0	0	0
$Q_\tau = 0.128$	−4.02	6.10	−2.93	−5.87	0.83	−0.40	0.40	−1.63	−0.04
				$Fe^{III}-Ni^{II}$					
$Q_\tau = 0$[b]	−2.87	4.30	0	0	0	0	0	0	0
$Q_\tau = 0.128$	−2.59	4.12	−1.89	−3.78	0.86	−0.14	0.14	−1.14	−0.15
	−2.59[d]	−6.09[d]	0.77[d]	0[d]	0[d]	0[d]	−0.29[d]	−1.12[d]	0[d]

[a] Calculated with $Q_\tau = Q_\xi = Q_\eta = Q_\zeta = 0.128$ Å; values of the vibronic coupling parameters used in the calculations are specified in Figure 2, and those of the other parameters are specified in Figures 3 (Fe−Cu) and 5(Fe−Ni). [b] Parameter values for the $Fe^{III}-CN-M^{II}$ complexes without Jahn–Teller distortions on $[Fe(CN)_6]^{3-}$ ($Q_\tau = 0$) are included for the sake of comparison. Ground-state **g** tensors (normalized to a ground-state spin of $\pm 1/2$) are $g_{x,y} = 0$ and $g_z = 6.35$; to get the g values for the ground-state effective spin, the reported ones should be divided by 3. The angles between the direction of the large components of the **g** tensors and the x, y, and z axes of the global coordinate frame are 90° (x, y) and 0° (z). [c] For the calculation of the exchange Hamiltonian parameters, full configuration mixing between the ground-state spin multiplet and the electronically excited states was taken into account (in contrast to eq 10). [d] Parameter values of the exchange Hamiltonian which diagonalize the $\mathbf{D}_{12}$ tensor of the $Fe^{III}-Ni^{II}$ pair. The angles between the direction of the unique $\mathbf{D}_{12}$ component (−6.09 cm^{-1}) and the x, y, and z axes of the global coordinate frame are 23, 68, and 87°, respectively. Ground-state **g** tensors (normalized to a ground-state spin of $\pm 1/2$) are $g_{x,y} = 0$ and $g_z = 6.86$; to get the g values for the ground-state effective spin, the reported ones should be divided by 3. The angles between the direction of the large components of the **g** tensors and the x, y, and z axes of the global coordinate frame are 73° (x, y) and 25° (z).

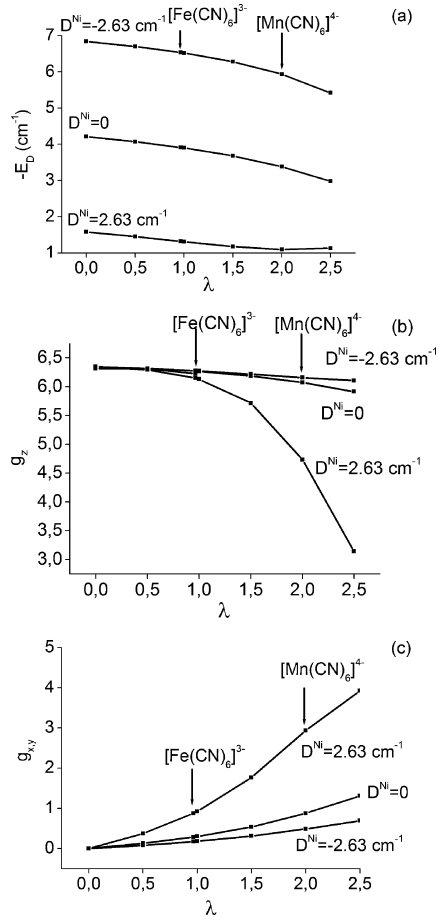

Figure 11. Effect of dynamic Jahn–Teller coupling due to the τ_{2g} trigonal modes on (a) the spin energy gap $-E_D$ and (b) the x and y and (c) z components of the **g** tensor of the $Fe^{III}-Ni^{II}$ pair. The dependence of the parameters on the vibronic coupling strength λ and the zero-field splitting of Ni^{II} (D_{Ni}) are shown; λ values for $[Fe(CN)_6]^{3-}$ and $[Mn(CN)_6]^{4-}$ are indicated by arrows. Values of the vibronic coupling parameters used are specified in Figure 2.

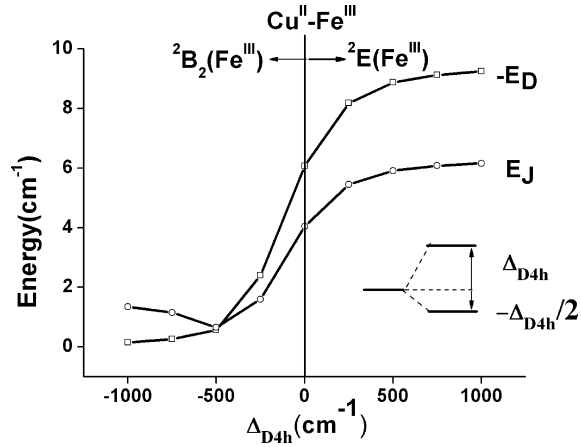

Figure 12. Dependence of the spin energy gap parameters $-E_D$ and E_J of an $Fe^{III}-Cu^{II}$ pair on the parameter $\Delta_{D_{4h}}$, which describes the splitting due to tetragonal strain created by the ligand L in a *trans*-$[Fe^{III}(CN)_2(L)_4]$ or a *trans*-$[Fe^{III}(CN)_4L_2]$ complex. The sign of $\Delta_{D_{4h}}$ is determined by the difference between the π-bonding characters of L and CN; for an amine ligand L without orbitals for π bonding, the dominating π back-bonding of CN^- should cause $\Delta_{D_{4h}}$ to be negative {positive} for *trans*-$[Fe^{III}(CN)_2(L)_4]$ {*trans*-$[Fe^{III}(CN)_4L_2]$}. Values of the parameters used for the plot are specified in Figure 3.

coincides with the Fe−CN−M linear bridge. The latter is described by eq 15 in terms of $\Delta_{D_{4h}}$, the energy for tetragonal splitting of the $^2T_{2g}$ ground term. This splitting yields either a ^2E_g or a $^2B_{2g}$ ground term, depending on the sign of $\Delta_{D_{4h}}$ ($\Delta_{D_{4h}} > 0$ or $\Delta_{D_{4h}} < 0$, respectively). As shown in Figure 12, both the magnetic anisotropy ($-E_D$) and the isotropic exchange energy (E_J) are greatly enhanced for tetragonal strain that leads to a ^2E_g ground state on Fe^{III}. In contrast, both parameters are strongly quenched if a nondegenerate $^2B_{2g}$ ground state becomes separated from a ^2E_g excited state with an energy gap $\Delta_{D_{4h}}$ comparable to or larger than the spin–orbit coupling energy $3\zeta/2$.

$$\mathbf{H}^{s}_{D_{4h}} = \begin{bmatrix} -\frac{\Delta_{D_{4h}}}{2} & 0 & 0 \\ 0 & -\frac{\Delta_{D_{4h}}}{2} & 0 \\ 0 & 0 & \Delta_{D_{4h}} \end{bmatrix} \qquad (15)$$

5. Comparison with Experimental Data

A large number of oligonuclear cyanometalates containing Cu^{II} or Ni^{II} combined with low-spin Fe^{III} and having ferromagnetic ground states have been synthesized and

Table 5. Spin Ground States (S), Exchange Coupling Constants (J in $\hat{H}_{exc} = -J\mathbf{S}_1\cdot\mathbf{S}_2$), Calculated ($U$) and Experimental ($U_{eff}$) Effective Energy Barriers for Reorientation of the Magnetization, and Zero-Field Splitting Parameters (D and E) in Trinuclear $Fe^{III}-Ni^{II}-Fe^{III}$, Rectangular $(Fe^{III})_2(M^{II})_2$, Trigonal Bipyramidal $(M_1)_2(M_2)_3$ ($M_1 = Fe^{III}$, Ni^{II}; $M_2 = Cu^{II}$, Ni^{II}, Fe^{III}), and Heterocubane $Ni^{II}_4Fe^{III}_4$ Exchange Complexes[a]

complex	S	$J(M_1-M_2)$	U_{eff}	U	D	E	ref
cis-$Ni^{II}(NC)_2Fe^{III}_2$[j]	2	9.3	8	13.7	−3.4[b]		1
trans-$Ni^{II}(NC)_2Fe^{III}_2$[k]	2	1.7	−	−	−		1
$Fe^{III}_2(CN)_4Cu^{II}_2$[l]	2	12.6	−	−	−		5
$Fe^{III}_2(CN)_4Cu^{II}_2$[m]	3[c]	9.8	−	−	−		6
$Fe^{III}_2(CN)_4Ni^{II}_2$[n]	3	10.6	−	35.8	−3.98[d]		7
$Fe^{III}_2(CN)_4Cu^{II}_2$[o]	2	23.8	−	−	−		8
$Fe^{III}_2(CN)_4Cu^{II}_2$[p]	2	2.76	−	4.6	−1.15[d,e]		8
$Fe^{III}_2(CN)_4Ni^{II}_2$[q]	3	9.04	18.9	34.65	−3.85		8
$Fe^{III}_2(CN)_6Cu^{II}_3$[r]	$^5/_2$	17.0	16	34[f]	−5.7	0.0014	9
$Fe^{III}_2(CN)_6Cu^{II}_3$[s]	$^5/_2$	6.9	−	2.9[f]	−0.49[d]	0.094	10
$Fe^{III}_2(CN)_6Cu^{II}_3$[t]	$^5/_2$	15.84	−	14.34[f]	−2.39[d]	0.36	10
$Fe^{III}_2(CN)_6Ni^{II}_3$[u]	4	10.6	−	−	−[g]	−	11
$Fe^{III}_2(CN)_6Ni^{II}_3$[v]	4	8.6	−	−	−[h]	−	12
$Fe^{III}_2(CN)_6Ni^{II}_3$[w]	4	6.6	−	−	−[i]	−	12
$Fe^{III}_2(CN)_6Ni^{II}_3$[x]	4	10.8	−	−	−1.7[d]	0.02	2
$Ni^{II}_2(NC)_6Fe^{III}_3$[y]	$^7/_2$	9.7	−	−	−0.8[d]	−	3
$Fe^{III}_4(CN)_{12}Ni^{II}_4$[z]	6	12.7		7.93	−0.22[d]		4
$Fe^{III}_4(CN)_{12}Ni^{II}_4$[aa]	6	12.0		14.0	−0.39[d]		10

[a] All energies in cm^{-1}. [b] Calculated from U using the equation $U = S^2|D|$ for integer spins S. [c] Coupling of two $S = 1$ Cu^{II} iminonitroxide units with two $s = {}^1/_2$ low-spin Fe^{III} centers. [d] From a fit to field-dependent magnetization. [e] Inaccurate because of the proximity of the excited $S = 1$ spin state, which is only 2.76 cm^{-1} above the ground state. [f] Calculated from D using the equation $U = (S^2 - {}^1/_4)|D|$ for half-integer spins S. [g] Positive zero-field splitting parameter of 2.4 for Ni^{II}.[11] [h] Positive zero-field splitting parameter of 8.8 for Ni^{II}.[12] [i] Positive zero-field splitting parameter of 5.8 for Ni^{II}.[12] [j] $\{[(pzTp)Fe^{III}(CN)_3]_2[Ni^{II}(bipy)_2]\}\cdot 2H_2O$; bipy = 2,2′-bipyridine, pzTp = tetra(pyrazol-1-yl)borate. [k] $\{[(pzTp)Fe^{III}(CN)_3]_2[Ni^{II}(L)]\}\cdot {}^1/_2MeOH$; L = 1,5,8,12-tetraazadodecane. [l] $[Fe^{III}_2Cu^{II}_2(\mu\text{-}CN)_4(bpy)_6](PF_6)_6\cdot 4CH_3CN\cdot 2CHCl_3$. [m] $[Fe^{III}_2Cu^{II}_2(\mu\text{-}CN)_4(dmbpy)_4(impy)_2](ClO_4)_6\cdot 4CH_3OH\cdot 4H_2O$; dmbpy = 4,4′-dimethyl-2,2′-bipyridine, impy = 2-(2-pyridyl)-4,4,5,5-tetramethyl-4,5-dihydro-1*H*-imidazolyl-1-oxy. [n] $\{[Tp^*Fe^{III}(CN)_3Ni^{II}(DMF)_4](OTf)_2\}\cdot 2DMF$; Tp* = hydridotris(3,5-dimethylpyrazol-1-yl)borate, OTf = trifluoromethanesulfonate. [o] $[(Tp)Fe(CN)_3Cu(Tp)]_2\cdot 2H_2O$; Tp = tris(pyrazolyl)hydroborate. [p] $[(Tp)Fe(CN)_3Cu(bpca)]_2\cdot 4H_2O$; bpca = bis(2-pyridylcarbonyl)amidate anion. [q] $[(Tp)Fe(CN)_3Ni(tren)]_2(ClO_4)_2\cdot 2H_2O$; tren = tris(2-aminoethyl)amine. [r] $[Tp_2(Me_3tacn)_3Cu_3Fe_2(CN)_6](ClO_4)_4\cdot 2H_2O$; Me_3tacn = *N*,*N*′,*N*″-trimethyl-1,4,7-triazacyclononane. [s] $[(Tp^{4Bo})_2(Me_3tacn)_3Cu_3Fe_2(CN)_6](ClO_4)_4\cdot 5H_2O$; Tp^{4Bo} = tris(indazolyl)hydroborate. [t] $[(pzTp)_2(Me_3tacn)_3Cu_3Fe_2(CN)_6](ClO_4)_4\cdot 4H_2O$. [u] $\{[Ni(bpm)_2]_3[Fe(CN)_6]_2\}\cdot 7H_2O$; bpm = bis(1-pyrazolyl)methane. [v] $\{[Ni(tmphen)_2]_3[Fe(CN)_6]_2\}\cdot 14H_2O$; tmphen = 3,4,7,8-tetramethyl-1,10-phenanthroline. [w] $[Ni(bpy)_2(H_2O)]\{[Ni(bpy)_2]_2[Fe(CN)_6]_2\}\cdot 12H_2O$. [x] $[Tp_2(cyclen)_3Ni_3Fe_2(CN)_6](BF_4)_4$; Tp = hydrotris(1-pyrazolyl)borate, cyclen = 1,4,7,10-tetraazacyclododecane. A possible alternative set with $D = 2.6$ cm^{-1} and $E = 0.18$ cm^{-1} has been reported. [y] $[(Tp)_3(Tpm^{Me})_2Fe^{III}_3Ni^{II}_2(CN)_9](ClO_4)\cdot 15H_2O$; Tpm^{Me} = tris(3,5-dimethyl-1-pyrazolyl)methane. [z] $[(pzTp)Fe^{III}(CN)_3]_4[Ni^{II}L]_4(OTf)_4\cdot 10DMF\cdot Et_2O$; L = 2,2,2-tris(pyrazolyl)ethanol. [aa] $[(pzTp)_4(phen)_4Ni_4Fe_4(CH_3OH)_4(CN)_{12}](ClO_4)_4\cdot 4H_2O$.

characterized (Table 5). These include trinuclear Fe_2Ni complexes containing *trans*- and *cis*-$(Fe-CN)_2-Ni$ units,[1] heterometallic square-shaped M_2Fe_2 complexes,[5–8] trigonal bipyramidal M_3Fe_2 structures,[2,3,9–12] and heterometallic Ni_4Fe_4 cubane complexes.[4,10] Effective thermal barriers U_{eff} for the reversal of magnetization, obtained by temperature-dependent ac susceptibility measurements, indicate that only three of the systems, *cis*-Fe_2Ni,[1] Fe_2Ni_2,[8] and Fe_2Cu_3,[9] display SMM behavior. In nine other systems, a negative D value was deduced from a fit to field-dependent magnetizations (Table 5). Despite having similar cluster topologies and the same type of ferromagnetic ground state, seven other systems with integer-spin ground states (*trans*-Fe_2Ni, three Fe_2Cu_2 compounds, and three Fe_2Ni_3 compounds) demonstrated no SMM behavior. What is the reason for these striking differences?

We have performed calculations of the spin levels of clusters containing Fe^{III} and Cu^{II} or Ni^{II}, based on the vector coupling scheme presented in the Theory section; the topologies and coordinate systems used in these calculations are specified in Figure 13. The exchange coupling tensors of $Fe^{III}-Cu^{II}$ and $Fe^{III}-Ni^{II}$ pairs having linear Fe−CN−M bridges and no angular distortion of $[Fe(CN)_6]^{3-}$ assume a simple form in which only two exchange parameters (D and J) are needed in order to describe each pair. The local **g** and **D** tensors of the dinuclear units can be coupled to yield the spin levels and magnetic properties of entire magnetic clusters. Ground-state spin multiplicities, spin gap energies (relative to the ground state) and multiplicities of the lowest

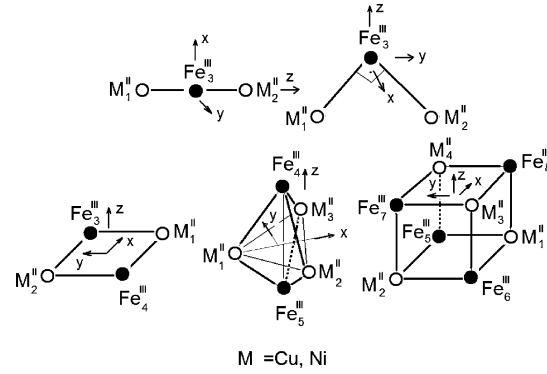

Figure 13. Oligonuclear spin clusters based on $Fe^{III}-M^{II}$ pairs with linear $Fe^{III}-CN-M^{II}$ bridges, for which the data in Tables 6 and 7 were calculated.

excited spin states, and magnetizations as a function of direction and the magnitude of the applied magnetic field [in the low-field ($B = 0.2$ T) and high-field ($B = 7$ T) limits] are provided in Table 6. Values of the **g** tensor for spin clusters having a doubly degenerate (bistable) ground state are listed in Table 7. The calculations yielded a sizable spin gap energy, comparable in magnitude to that reported[9] for Cu_3Fe_2 ($-D = 5.7$ cm^{-1}, Table 5) for only three of the systems, namely, linear Fe−Ni, *trans*-Cu−Fe−Cu, and Ni−Fe−Ni. In these examples, a large, field-independent magnetization along the easy axis (oriented in the z direction) and almost zero perpendicular magnetization were obtained, and the calculated **g**-tensor components (Table 7) reflect this anisotropy. A very small spin energy gap was calculated for

Table 6. Energies (in cm^{-1}) and Multiplicities of the Ground[a] and Lowest-Excited Spin States and Field-Dependent Ground-State Magnetizations[b] (in Bohr Magnetons) of Highly Symmetric Oligonuclear Model Spin Clusters Built Up from $Fe^{III}-M^{II}$ Cyanide-Bridged Pairs[c,d]

		lowest-excited spin state		$B = 0.2$ T			$B = 7$ T		
complex	ground-state multiplicity	energy	multiplicity	M_x	M_y	M_z	M_x	M_y	M_z
CuFe	1	53	1	0.11	0.11	1.02	1.74	1.74	1.86
NiFe	2	4.30	2	0.14	0.14	**3.16**	2.95	2.95	**3.16**
trans-Cu_2Fe	2	6.22	2	0.28	0.28	**2.85**	2.61	2.61	**2.85**
trans-Ni_2Fe	2	4.30	4	0.24	0.24	**5.46**	5.00	5.00	**5.46**
cis-Cu_2Fe	2	0.64	2	1.22	2.24	2.24	2.68	2.89	2.89
cis-Ni_2Fe	4	1.78	4	0.80	4.33	4.33	5.10	5.34	5.34
Cu_2Fe_2	1	1.29	1	0.67	0.67	0.17	3.70	3.70	3.24
Ni_2Fe_2	4	1.93	4	4.67	4.67	0.73	6.21	6.21	5.59
Cu_3Fe_2	2	1.11	2	2.78	2.78	2.32	4.67	4.67	4.47
Ni_3Fe_2	1	0.35	3	3.92	3.92	1.57	8.31	8.31	8.37
Cu_4Fe_4	1	2.37	2	1.08	1.08	1.08	7.23	7.23	7.23
Ni_4Fe_4	4	0.21	12	9.23	9.23	9.23	12.20	12.20	12.20

[a] Energies of the spin ground states are set at zero. [b] Magnetizations M_x, M_y, and M_z are defined with respect to the global Cartesian axes established for each model complex as shown in Figure 13. [c] Data for the constituent dinuclear $Fe^{III}-M^{II}$ units are given for the sake of comparison. Calculations have been done using the pair model, adopting a regular (nondistorted) octahedral $[Fe(CN)_6]^{3-}$ unit, assuming fourfold (pseudo)symmetry of each M−NC−Fe bridge, and coupling the local $\mathbf{g}_i$ and $\mathbf{D}_{ij}$ tensors of each pair to the tensors of the total cluster. Values of the isotropic spin coupling energy J and the parameter D that defines the local anisotropy $\mathbf{D}$ tensor for each M−Fe pair were −4.49 and 5.93 cm^{-1}, respectively, for $Fe^{III}-Cu^{II}$ and −2.87 and 4.30 cm^{-1}, respectively, for $Fe^{III}-Ni^{II}$; other parameter values for Fe were $k = 0.79$ and $\zeta = 345$ cm^{-1}. Values of the $\mathbf{g}$-tensor components were $g_x = g_y = g_z = 2.30$ for Ni^{II}, $g_x = g_y = 2.18$ and $g_z = 2.00$ for CuFe and Cu_2Fe, $g_x = g_y = 2.05$ and $g_z = 2.25$ for Cu_3Fe_2 [with the directions of $g_{ix,y}$ and g_{iz} taken to be within and perpendicular to, respectively, the $Fe_4-Cu_i-Fe_5$ ($i = 1, 2, 3$) plane], and $g_x = g_y = g_z = 2.116$ for Cu_2Fe_2 and Cu_4Fe_4. [d] Bold print indicates a system having a field-independent magnetic moment and strong anisotropy.

Table 7. Values of $\mathbf{g}$-Tensor Components[a] for Oligonuclear Model Spin Clusters Containing Fe^{III} and Cu^{II} or Ni^{II} and Having Doubly Degenerate (Bistable) Spin Ground States[b]

spin cluster	g_x[c]	g_y[c]	g_z[c]
NiFe	0	0	6.351
trans-Cu_2Fe	0.379	0.379	5.693
trans-Ni_2Fe	0	0	10.920
cis-Cu_2Fe	2.294	3.860	3.860
Cu_3Fe_2	4.862	4.862	4.160

[a] See Figure 13 for the definition of the global Cartesian axes x, y, and z for each spin cluster. [b] See Table 4 for definitions and numerical values of the local Ni^{II} and Cu^{II} $\mathbf{g}$ tensors. [c] Values of the $\mathbf{g}$-tensor components are given with respect to an $s' = {}^1/_2$ effective spin; to get the $\mathbf{g}$-tensor components of the actual spin, the values from the table must be divided by the total number of $s = {}^1/_2$ spins (i.e., by 3 for NiFe and *trans*- and *cis*-Cu_2Fe or 5 for *trans*-Ni_2Fe and Cu_3Fe_2).

Table 8. Deviations ($\delta\alpha$, in deg) of the $C-Fe^{III}-C$ Angles α from 90° (the Value Corresponding to a $[Fe(CN)_6]^{3-}$ Complex without Angular Distortions) and Deviations ($\delta\beta$ and $\delta\gamma$, in deg) of the $Fe^{III}-C-N$ and $C-N-M^{II}$ Angles β and γ, Respectively, from 180° (the Value Corresponding to Ideally Linear Fe−C−N−M Units), As Derived from Structural Data on Cu_3Fe_2[9] and Ni_3Fe_2[2] Spin Clusters

Fe−M pair[a]	$\delta\alpha(C-Fe^{III}-C)$	$\delta\beta(Fe^{III}-C-N)$	$\delta\gamma(C-N-M^{II})$
		Cu_3Fe_2	
Fe_4-Cu_1	−3.1	−2.4	−10.4
Fe_4-Cu_2	−0.8	−3.1	−7.3
Fe_4-Cu_3	−1.8	−3.6	−8.8
Fe_5-Cu_1	−3.6	−3.2	−6.0
Fe_5-Cu_2	−3.4	−1.9	−8.3
Fe_5-Cu_3	0.9	−2.8	−8.5
		Ni_3Fe_2	
$Fe_4-Ni_{1,2,3}$	−1.9	−0.8	−4.2
$Fe_5-Ni_{1,2,3}$	0.5	−0.9	−10.8

[a] See Figure 13 for definitions of atom labels.

all of the other systems. As the field-dependent ground-state magnetization values (Table 6) indicate, there is a strong effect of the magnetic field on the ground state via mixing of the closely spaced ground and excited spin states. There is a cancellation of the large anisotropies of the individual $Fe^{III}-Cu^{II}$ and $Fe^{III}-Ni^{II}$ pairs when their local $\mathbf{D}_{12}$ and $\mathbf{g}$ tensors are coupled in magnetic clusters of high symmetry, such as the M_3Fe_2 and M_4Fe_4 complexes. Magnetic anisotropies for Cu_3Fe_2, in both the magnetization and the $\mathbf{g}$ tensors, were found to be small. This contrasts with the high anisotropy measured in the Cu_3Fe_2 SMM.[9] Parameters for angular distortions within the bridging $Fe(CN)_3$ site [i.e., $\delta\alpha$, the deviations of the C−Fe−C angles α from 90°] and for distortion of the Fe−CN−M bridges from linearity [i.e., $\delta\beta$ and $\delta\gamma$, the deviations of the Fe−C−N and C−N−M angles β and γ, respectively, from 180°] are listed in Table 8. With a Jahn–Teller coupling mechanism, the parameters of the exchange Hamiltonian strongly depend on the distortions $\delta\alpha$, as reflected by the energy $-E_D$ (see Figures 9 and 10a). These distortions are very large for Fe_2M_3 (see Table 8) and are therefore expected to strongly influence the spin levels and magnetic properties. However, the variation of $\delta\alpha$ is irregular and does not allow the application of the simple symmetry-based Jahn–Teller description. Therefore, a full calculation using the exact angular geometry in each magnetic cluster is mandatory when modeling the magnetic data.

In addition to $\delta\alpha$, the geometry of the Fe−CN−M bridge is expected to affect the anisotropy. Because the $Fe^{III}-CN$ bond is stronger than the $CN-M^{II}$ bond, deviations ($\delta\gamma$) of the C−N−M angle due to angular strain and packing forces are expected to be larger than those ($\delta\beta$) of the Fe−C−N angle. This expectation is supported by the data in Table 8. It has been shown experimentally[1] and by DFT calculations[125] (see also ref 126) that nonzero values of $\delta\gamma$ decrease the overlap of the magnetic orbitals and reduce the exchange coupling energy $J(^2E)$. In contrast, $J(^2B_2)$ is expected to increase in magnitude. This must be taken into account in quantitative studies.

From the comparison between the computational results for model clusters of high symmetry and the reported magnetic data, we conclude that symmetry reduction (as revealed by the reported angular distortions) plays a different

(125) Zhang, Y.-Q.; Luo, C.-L.; Yu, Z. *New J. Chem.* **2005**, *29*, 1285.

role in *trans*-M_2Fe than in M_3Fe_2 and M_4Fe_4 complexes. Angular distortions reduce the magnetic anisotropy of the linear Cu−Fe−Cu and Ni−Fe−Ni structures but induce anisotropy in the higher-symmetry M_3Fe_2 (D_{3h}) and M_4Fe_4 (T_d) clusters. This conclusion is supported by experimental data on highly symmetric $Cu^{II}_6Fe^{III}_8$ cyanide-bridged face-centered cubic clusters that demonstrate SMM behavior.[13,18]

A large and accidental ground-state degeneracy of 4 is predicted for the regular *cis*-Ni_2Fe, Ni_2Fe_2, and Ni_4Fe_4 spin clusters having C_{2v}, D_{2h}, and T_d symmetries, respectively, and an even larger degeneracy (12) is found in the lowest excited state of Fe_4Ni_4, which lies only 0.21 eV above the ground state. When coupled to angular distortions, these degenerate ground states can be modified by antisymmetric exchange, which can be very large even for small values of $\delta\alpha$ (see Table 4). This might help to explain the atypical relaxation behavior reported for the Fe_4N_4 SMM.[4]

The effect of tetragonal strain (Figure 12) is manifested by bulk magnetic susceptibility, ESR, and Mössbauer data on the cyanide-bridged $Fe^{III}-Cu^{II}$ heterobinuclear complex in $[Fe(P)CNCu(N_4)](ClO_4)_2\cdot 3H_2O$ [P = α,α,α,α-tetrakis(*o*-nicotinamidophenyl) porphyrin].[63] Stabilization of the non-degenerate $^2B_{2g}$ ground state of Fe^{III} (negative $\Delta_{D_{4h}}$) and the small positive value of $J(B_2)$ lead to an $S' = 1$ ground state and an $S' = 0$ excited state that are estimated by EPR to be separated by only 0.25 cm^{-1}. Using the DFT values for $J(E)$ and $J(B_2)$, we have been able to reproduce this energy gap with a strain energy of $\Delta_{D_{4h}} = -1000$ cm^{-1}. Reported small values of the anisotropic and antisymmetric exchange parameters extracted from a simulation of the ESR spectrum nicely manifest the quenching of orbital momenta due to lifting of the orbital degeneracy of the $^2T_{2g}$ ground state of Fe^{III}. However, subtle effects arising from the coordination geometry of the Fe^{III} site may tune the anisotropic splitting of the $S' = 1$ sublevels over a wide range, leading to a spin-singlet ground state ($M_s' = 0$) and the absence of an EPR signal, as reported for the CN^- derivative of the oxidized form of the enzyme cytochrome oxidase, which has a pair of ferromagnetically coupled Cu^{II} and low-spin Fe^{III} sites and a similar $S' = 1$ ground state.[61,62]

6. Conclusions

1. A large magnetic anisotropy having an easy axis of magnetization along the cyanide bridge is predicted for $Fe^{III}-M^{II}$ (M = Cu, Ni) pairs with linear $Fe^{III}-CN-M^{II}$ bridging geometry and regular $[Fe(CN)_6]^{3-}$ octahedra. It arises from the orbital angular momentum in the $^2T_{2g}$ ground state of $[Fe(CN)_6]^{3-}$, which is transmitted to the spin ground state of the cluster by an orbital-dependent exchange mechanism. Enhancement of the exchange anisotropy is predicted to occur when it is combined with the single-ion anisotropy of Ni^{II} with a negative sign of D (leading to an $M_s = \pm 1 < M_s = 0$ splitting of the $S = 1$ ground state of Ni^{II}). This implies that the $Ni^{II}L_6$ octahedra are tetragonally compressed with a tetragonal axis aligned along the bridge.

2. In contrast to the Mn^{III}-based SMM,[127–129] Jahn–Teller coupling is not always favored for SMMs in spin clusters composed of $Fe^{III}-Cu^{II}$ and $Fe^{III}-Ni^{II}$ cyanide-bridged exchange-coupled pairs. Both Cu^{II} and Fe^{III} are Jahn–Teller active (for Fe^{III}, the Jahn–Teller coupling is relatively small but on the same order of magnitude as the spin–orbit coupling interaction). A trigonal distortion of as little as 2−3° in the $[Fe(CN)_6]^{3-}$ site is able to destroy the magnetic anisotropy, i.e., to reduce the spin anisotropy gap energy ($-E_D$ or U) in both the $Fe^{III}-Cu^{II}$ and $Fe^{III}-Ni^{II}$ pairs (Figures 9 and 10a, respectively). This is also the case in *trans*-Cu−Fe−Cu and -Ni−Fe−Ni complexes. Therefore, in the synthesis of new SMM materials, it is necessary to pay attention to the angular geometry and electronic structure of the Fe^{III} site, as revealed by absorption spectra due to d−d transitions. The Fe−CN bond is strong, and it is expected that Fe−CN distortions are less important. However, this may change for cyanide complexes having different ligands in the coordination sphere of Fe^{III} {e.g., in magnetic clusters composed of the $Fe(CN)_3$ units in $[Fe(Tp)(CN)_3]^-$ [Tp = hydrotris(pyrazolyl)borate], which impose a trigonal geometry,[2,9] and in the $[Fe(P)CN-Cu(N_4)]^{2+}$ [P = α,α,α,α-tetrakis(*o*-nicotinamidophenyl) porphyrin] complex,[63] which has tetragonal symmetry}. On the basis of t_{2g} orbital splittings (reported from EPR measurements[130] to be as large as 2900 cm^{-1}), it is expected that ancillary ligands can significantly modify the magnetic anisotropy. In particular, for cyanide complexes of Fe^{III} with ligands inducing a ^2E_g ground state, an increase of the magnetic anisotropy of the $Fe^{III}-CN-M^{II}$ pairs is predicted (as discussed in the section on strain).

3. Symmetry reduction is found to increase the magnetic anisotropy in spin clusters with high symmetry and partial or complete cancellation of the $Fe^{III}-Cu^{II}$ and $Fe^{III}-Ni^{II}$ local anisotropy tensors, as in M_3Fe_2 and M_4Fe_4.

4. The use of Ni^{II} instead of Cu^{II} complex precursors seems to be preferable; it yields more-regular M^{II} polyhedra and can add a negative single-ion anisotropy contribution to the SMM in certain cases. The latter effect can be under chemical control (i.e., enforcement of tetragonal compression rather than elongation in the NiL_6 precursor).

5. Dynamic Jahn–Teller coupling in hexacyanometalate $^2T_{2g}$ ground states is found to reduce the magnetic anisotropy to an extent that depends on the vibronic coupling strength. The effect is found to be weak with $[Fe(CN)_6]^{3-}$ but may become important with other hexacyanometalates, such as $[Mn(CN)_6]^{4-}$.

6. A procedure for computing the anisotropic exchange in oligonuclear clusters derived from $Fe^{III}-M^{II}$ pairs, which involves two parameters $J(E)$ and $J(B_2)$ that define a C_{4v} pseudosymmetry around each pair, has been proposed. Mixing of the magnetic orbitals due to deviations from this

(126) Alborés, P.; Slep, L. D.; Weyhermüller, T.; Rentschler, E.; Baraldo, L. M. *Dalton Trans.* **2006**, 948.
(127) Sessoli, R.; Gatteschi, D. *Angew. Chem., Int. Ed.* **2003**, *42*, 268–297.
(128) Anderlund, M. F.; Zheng, J.; Ghiladi, M.; Kritikos, M.; Rivière, E.; Sun, L.; Girerd, J.-J.; Åkermark, B. *Inorg. Chem. Commun.* **2006**, *9*, 1195.
(129) Oshio, H.; Nakano, M. *Chem.—Eur. J.* **2005**, *11*, 5178.
(130) Ray, M.; Mukherjee, R.; Richardson, J. F.; Buchanan, R. M. *J. Chem. Soc., Dalton Trans.* **1993**, 2451.

ideal geometry is taken into account by explicit consideration of the ligand field distortions around each Fe^{III} center. From such calculations, the isotropic constant J and the magnetic anisotropy described by the symmetric (**D**) and antisymmetric (**A**) tensors of each $Fe^{III}-M^{II}$ pair can be deduced and then added using a vector coupling scheme to yield exchange coupling tensors for the whole cluster. Qualitative discussions based on a high-symmetry concept related in this work to the Jahn–Teller effect can be extended to quantitative studies that focus on systems with strongly irregular $Fe(CN)_6^{3-}$ geometries or on low-spin Fe^{III}−cyanide complexes containing other ligands in the coordination sphere of Fe^{III}.

Acknowledgment. Financial support by the Deutsche Forschungsgemeinschaft(SPP 1137 "Molecular Magnetism") and the University of Heidelberg is gratefully acknowledged. We thank J. R. Long and B. M. Bartlett (Berkeley, CA) for a preprint of their work (ref 2) prior to publication, S. Piligkos (University of Copenhagen, Denmark) for computational help, and G. Rajaraman for stimulating discussions.

Supporting Information Available: Figures, text, and a table providing computational details and theoretical derivations mentioned in the text. This material is available free of charge via the Internet at http://pubs.acs.org.

IC701702X

(131) Atanasov, M.; Comba, P.; Förster, S.; Linti, G.; Malcherek, T.; Miletich, R.; Prikhod'ko, A. I.; Wadepohl, H. *Inorg. Chem.* **2006**, *45*, 7722.